

素子材料特論
第3授業

Li-ion電池負極(II)

ハードカーボン系負極

Anodic performance and their related factors

| Performances | Factors |
|---|--|
| Capacity | <ul style="list-style-type: none">• Sites for Li incorporation |
| Potential for charge and discharge | <ul style="list-style-type: none">• Reversibility of charge and discharge• Over potential• Non-electrochemical reaction |
| charge and discharge rate | <ul style="list-style-type: none">• Diffusivity of Li |
| Non-dischargeable charge | <ul style="list-style-type: none">• Reactivity of electrolyte• Reactivity of anode, hetero atomic groups, terminal C-H, edge carbon• Irreversible sites for Li incorporation |
| Cycle ability | <ul style="list-style-type: none">• Irreversible charge in structure |
| Safety | <ul style="list-style-type: none">• Stability of charged Li• Li-Carbon intercalation• Thermal stability of SEI• Reactivity of electrolyte |

Charge-Discharge Curves of Various Carbon Materials

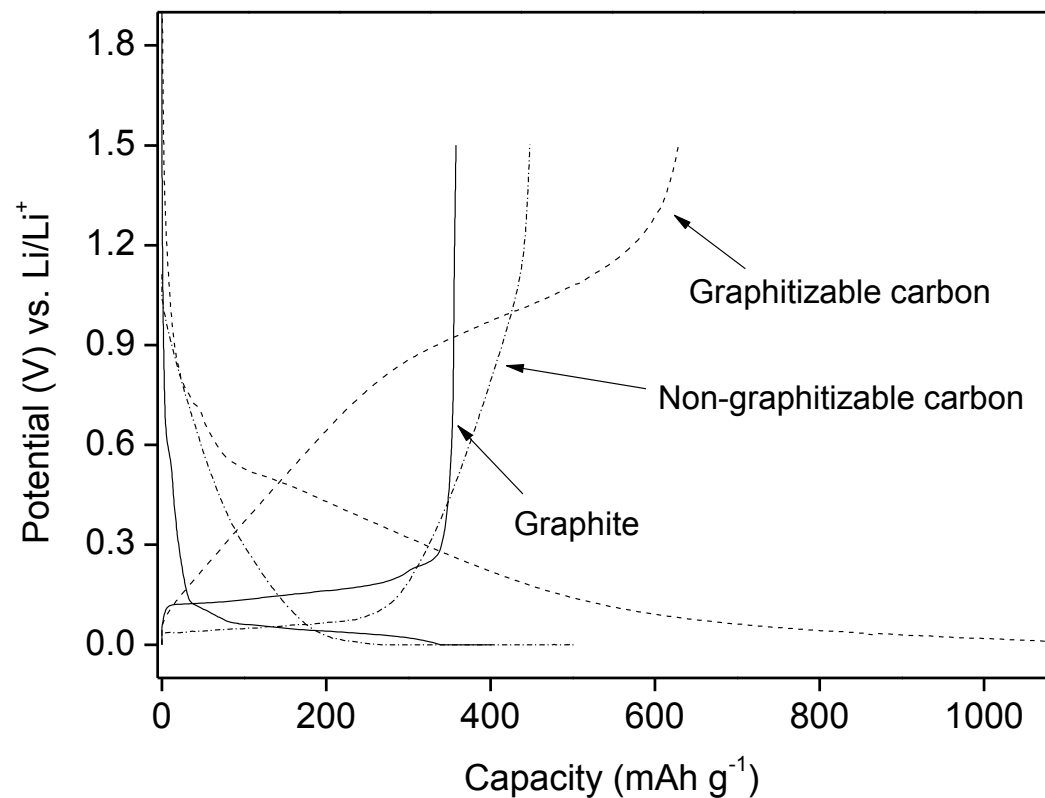
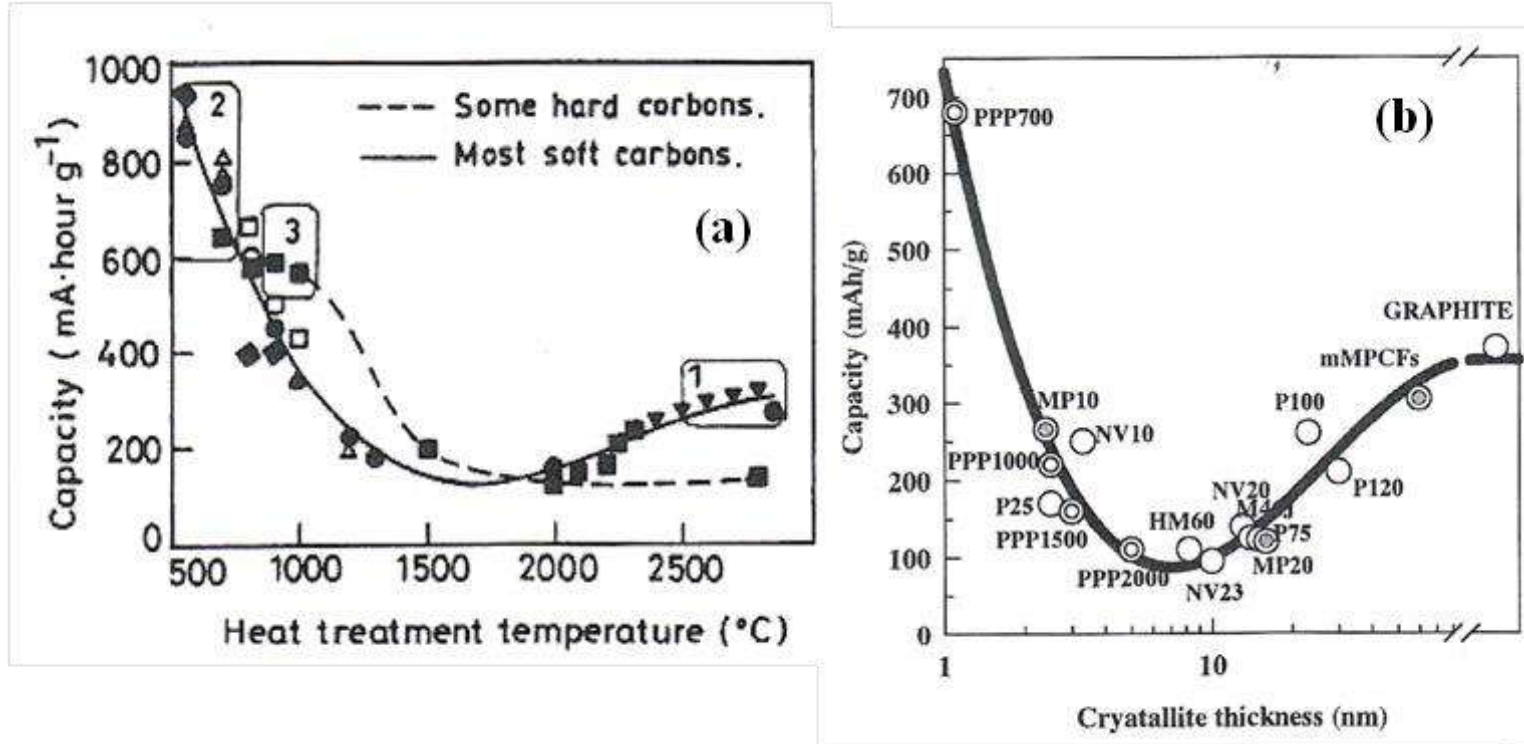


Figure 1-4. Charge-discharge profiles of representative carbon materials

Mechanisms for Lithium Insertion in Carbonaceous Materials



P100, P120, HM60, P25, P75, M46J ; Commercial MPCFs

MP10, MP20 ; MPCF HTT=1000, 2000 °C

NV10, NV20, NV23 ; Vapor grown carbon fiber HTT=1000, 2000, 2300 °C

PPP700, PPP1000, PPP1500, PPP2000 ; polyparaphenylene-based carbon

Figure 1-5. (a) Plot of reversible capacity for Li vs. HTT for a variety of carbon samples (□ hard carbon, ■ soft carbon), (b) Charge capacity as a function of the height of stacking (Lc002)

Characteristics of various materials

| | Precursor | Advantages | Disadvantages |
|---|--|---|--|
| Graphite (over 2800°C) | Natural graphite Artificial graphite MCMB Needle cokes VGCF | Low discharge potential (around 0.2V) Long cycle life | Low discharge capacity (372 mAh/g) High cost |
| Graphitizable carbon (600~800°C) | MCMB Meso phase pitch Green cokes | High capacity (700~1000mAh/g) Low cost | High discharge potential (around 1.0V) High irreversible capacity Poor cycle stability |
| Non-graphitizable carbon (1000~1400°C) | Thermosetting polymer Glassy carbon Coal Organic material Stabilized isotropic pitch | High capacity (400~700mAh/g) Low discharge potential (around 0.1V) Low cost | High irreversible capacity |

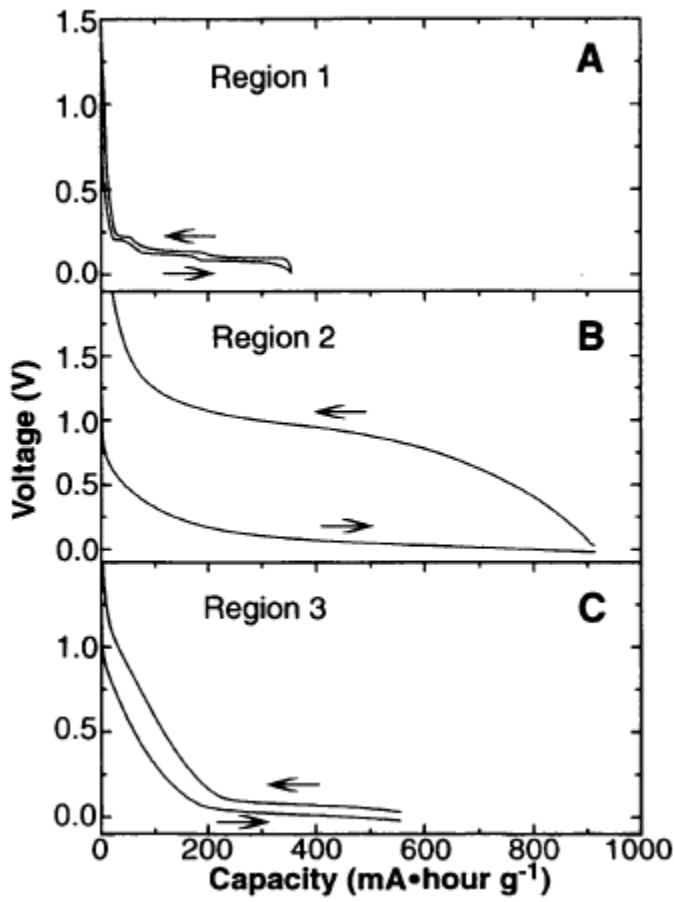


Fig. 2. Plots of voltage versus reversible capacity for the second charge-discharge cycle of representative carbon samples from regions 1, 2, and 3 of Fig. 1. (A) Synthetic graphite (Johnson-Matthey); (B) petroleum pitch (Crowley Tar Co.) heated to 550°C; (C) resole resin (Occidental Chemical Co.) heated to 1 000°C. Arrows designate the directions the curves are traversed as Li is added to (to the right) or removed from (to the left) the carbon samples.

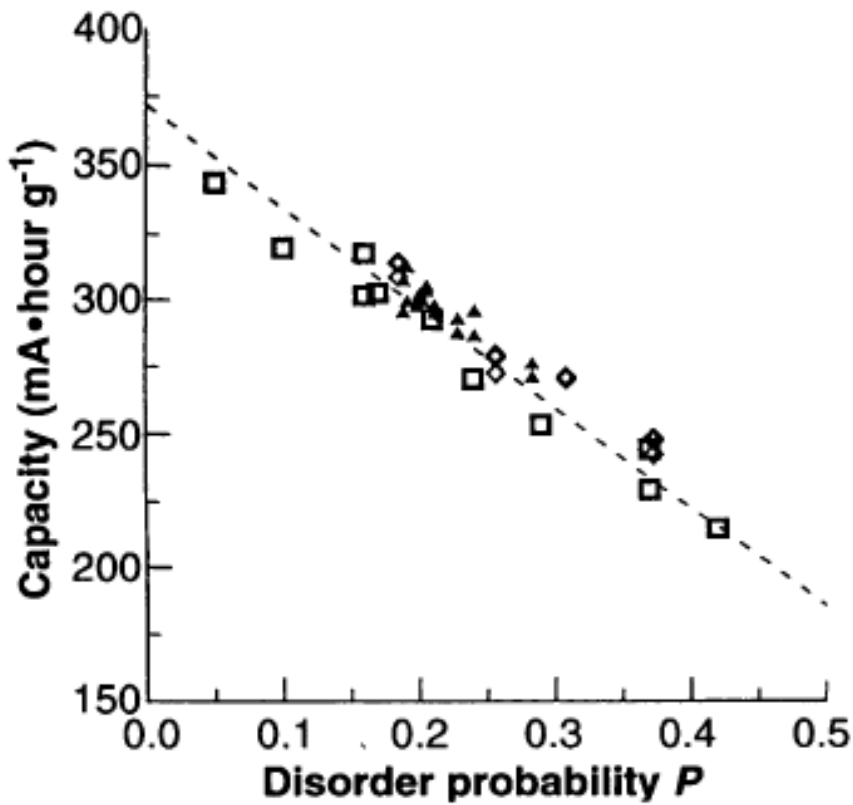
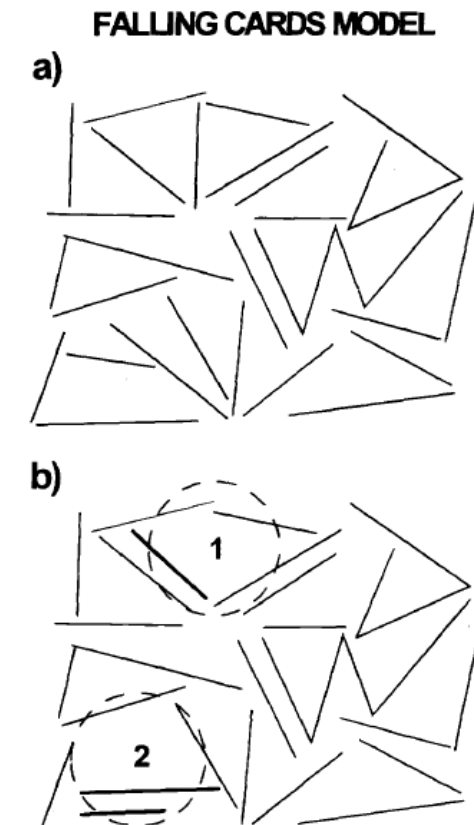
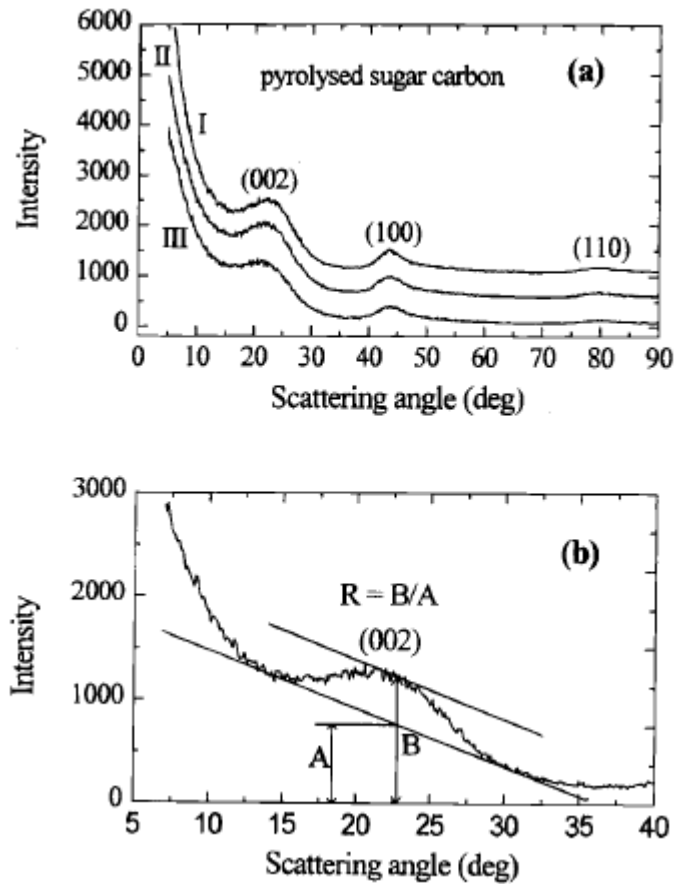


Fig. 3. Reversible capacity of region 1 carbons plotted as a function of the probability P of turbostratic disorder between adjacent carbon sheets. The line is the relation $Q = 372(1 - P)$, where Q is the capacity. For the purposes of this plot, samples corresponding to different symbols are equivalent.

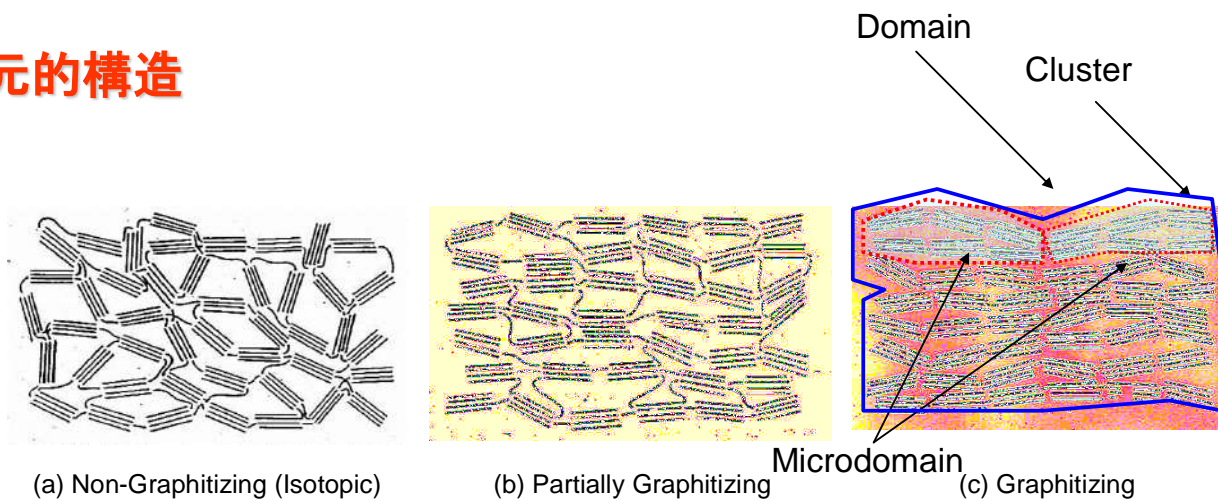
ハードカーボンの製造

- 原料: 難黒鉛化性前駆体
 - Biomass: Husk, Cellulose, Sugar, Rignin, Tree, Crab (Chichin), ...
 - Polymer: Phenol Resin, Unsaturated Resin, Epoxy Resin
 - Pitch: Isotropic Pitch and Coke
- 熱処理温度
 - 800~1400°C
- 構造
 - 難黒鉛化性カーボン

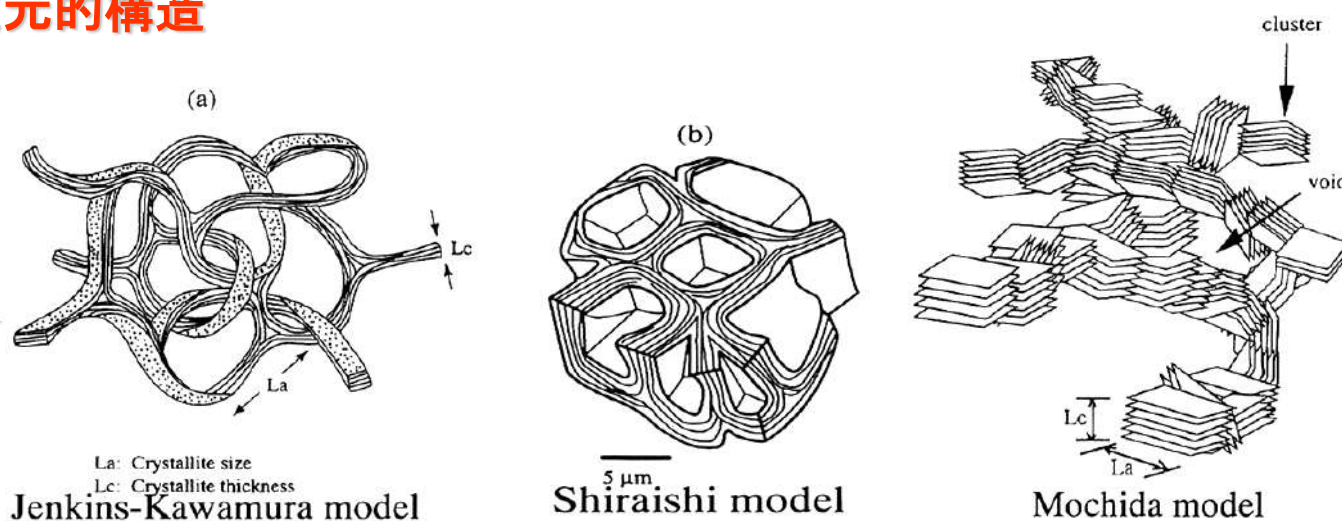


ハードカーボンの構造

2次元的構造



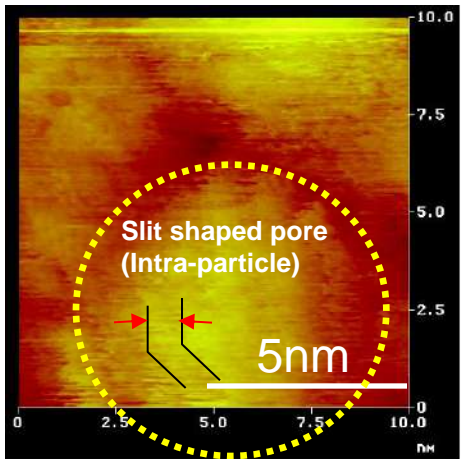
3次元的構造



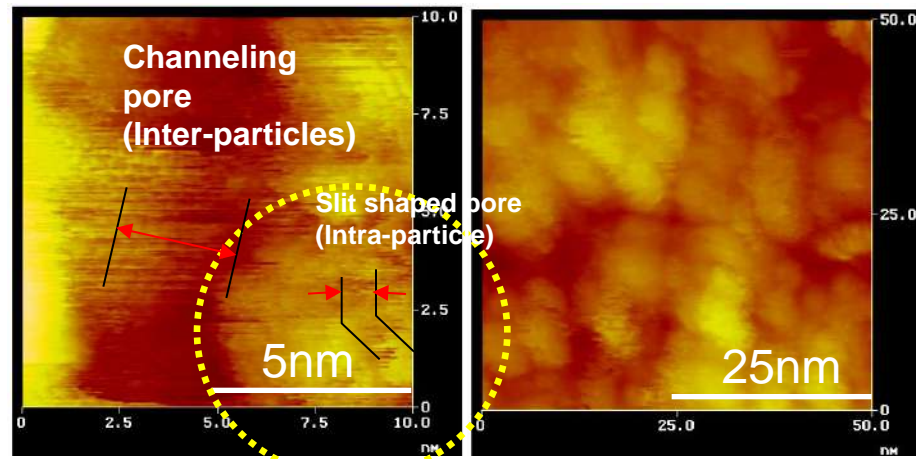
活性炭素繊維の微細構造

In order to remove oxygen containing functional groups for removing the heterogeneous effect of STM,
OG7A and OG20A were heat-treated at 800°C in a hydrogen atmosphere (H₂ / He =1/4).

OG7A-800H



OG20A-800H



♣ Vacant spaces between the two domains of OG20A are larger than that of OG7A.

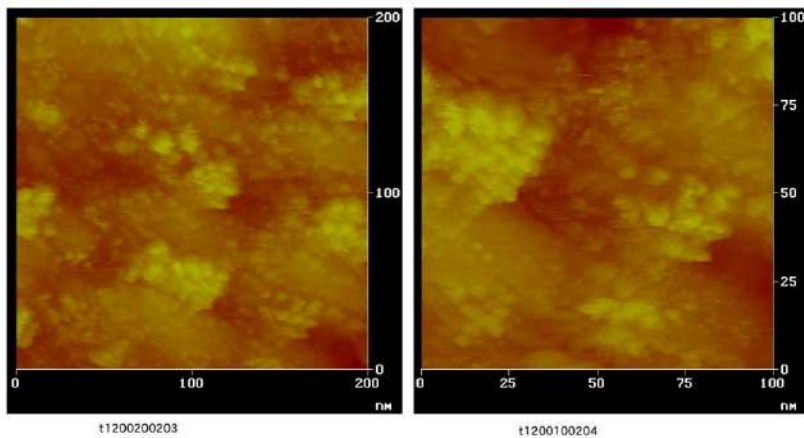
♣ Domain size of OG20A is a little smaller than that of OG7A.

♣ Slit type pores were observed in domains of OG7A and OG20A.

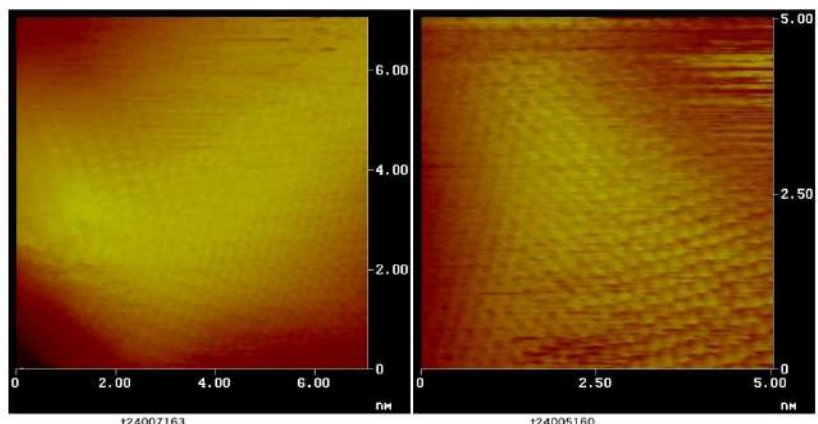
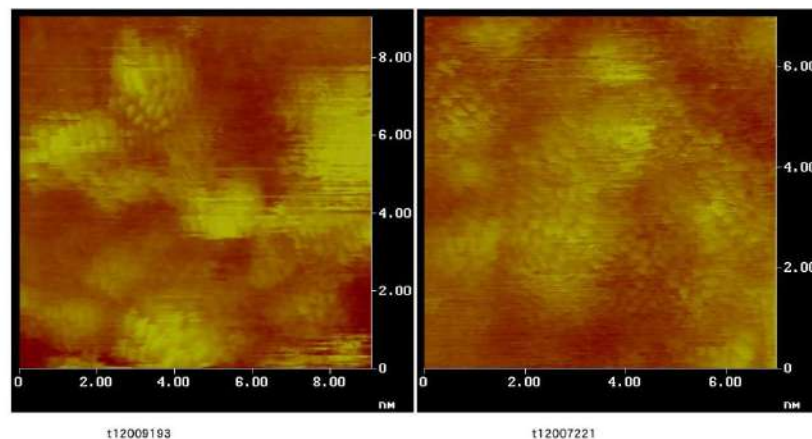
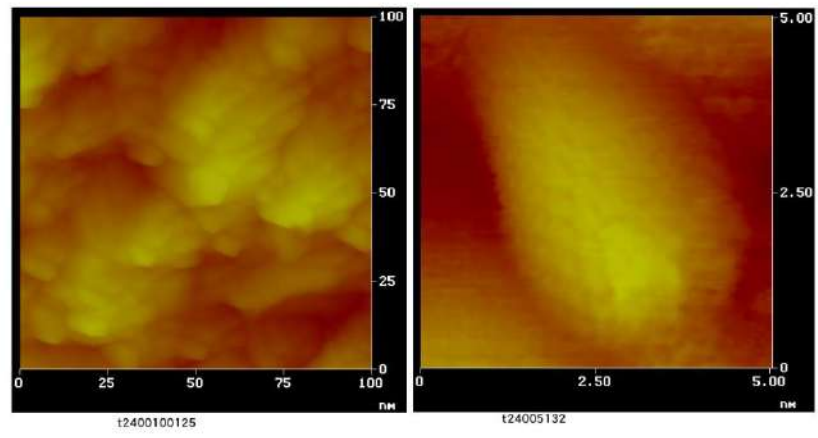
♣ It can be presumed that almost pores larger than 2nm nucleated by the inter-particle mechanism.

ガラス炭素の微細構造

1200°C



2400°C



ハードカーボンの長所と短所

- 長所
 - 高容量が可能
 - 安価(?)
 - 資源が豊富(?)
 - High rate property
 - Hybrid系材料が可能
 - 低温特性がよい。
 - 電解液のPC使用可能
- 短所
 - 低密度
 - 放電プロファイルがNon-platten
 - 不純物の除去が困難
 - 低1st cycle Coulombic efficiency
 - 低Cycle性
 - ...

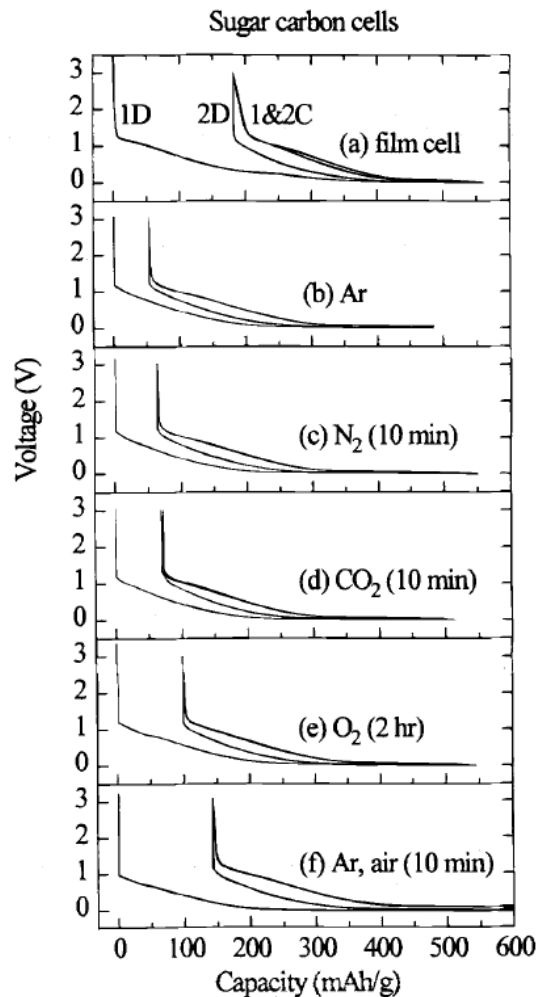


Fig. 2. Voltage profiles of sugar carbon/Li cells: (a) film electrode prepared in air and (b-f) tablet electrodes exposed to different gases as indicated.

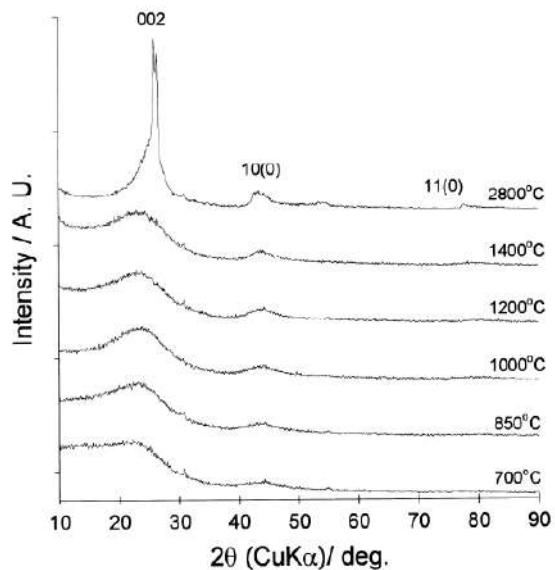


Fig. 1. Powder X-ray diffraction patterns of MNIP-derived carbonaceous materials. The sharp (002) diffraction lines appearing at $2\theta = 26$ and 26.5° in the 2800°C material come from the small portion of graphitized carbon.

Carbon 38 (2000) 995–1001

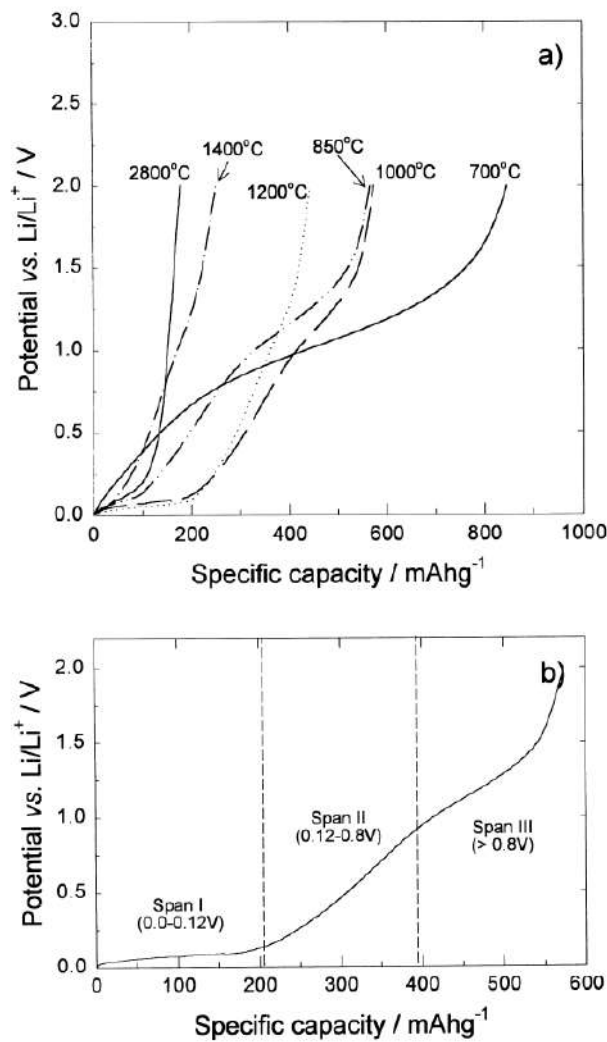
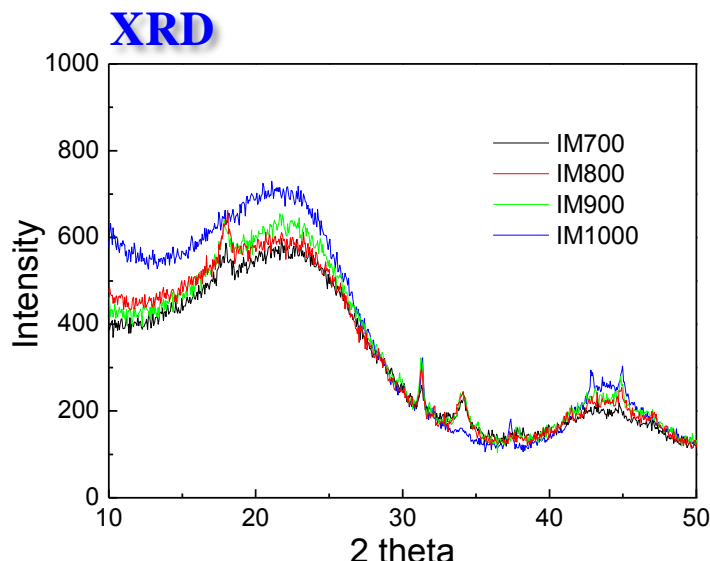


Fig. 2. Galvanostatic discharge curves of MNIP-derived carbons. The profile obtained with the 1000°C -prepared material is separately displayed in (b). Before the trace, the carbon electrodes were galvanostatically charged down to 0.0 V and further short-circuited with the Li counter electrode for 96 h. The current density was 30 mA g^{-1} (0.15 mA cm^{-2}). Note the change of slope at three different potential regions in (b).

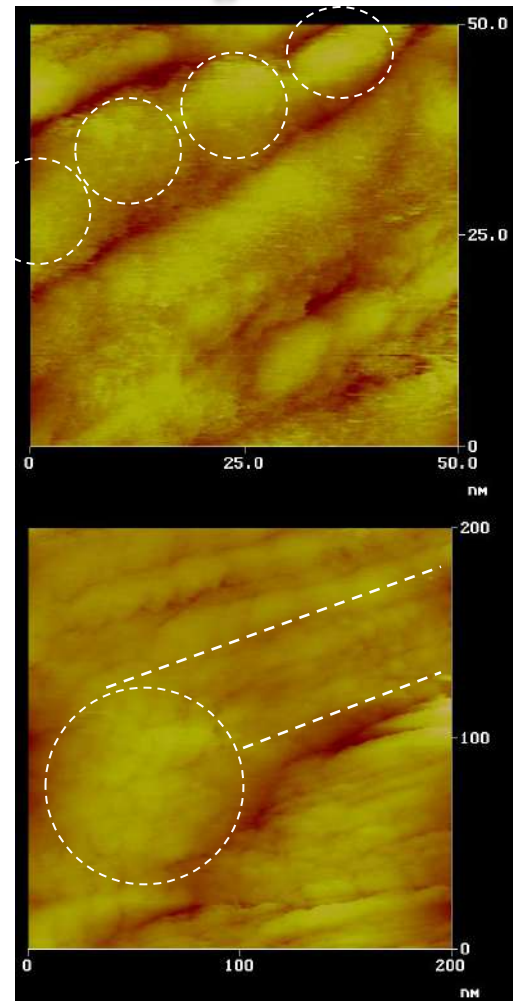
Hard Carbon from Indonesian Mangrove Char

Elemental analysis & Surface area

| | Elemental analysis (wt%) | | | | | S.A. (m ² /g) |
|---------|--------------------------|-----|------|------|-----|-----------------------------|
| | C | H | N | O | Ash | |
| IM | 70.6 | 3.6 | 0.38 | 23.7 | 1.7 | - |
| IM 700 | 89.4 | 1.0 | 0.72 | 582 | 3.1 | 318 |
| IM 800 | 90.0 | 0.8 | 0.74 | 5.5 | 3.0 | 19 |
| IM 900 | 91.0 | 0.6 | 1.17 | 4.3 | 3.0 | 3 |
| IM 1000 | 91.5 | 0.5 | 1.13 | 4.0 | 2.9 | 54 |



STM image of IM1000



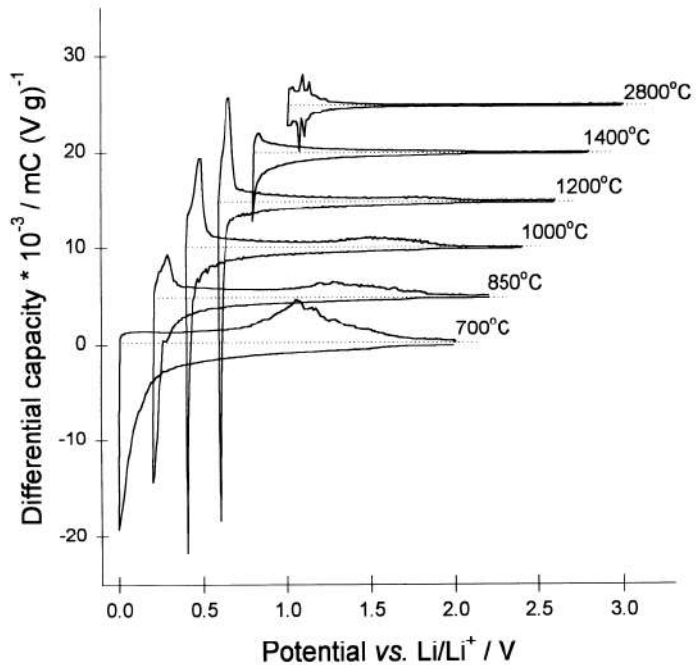


Fig. 4. EVS (electrochemical voltage spectroscopy) profiles obtained with the MNIP-derived carbons. In each profile, the upper traces correspond to discharging (Li^+ de-storage) and the bottom ones to charging (Li^+ storage). $I_{\text{threshold}} = 0.01 \text{ mA}$ and voltage step = 5 mV.

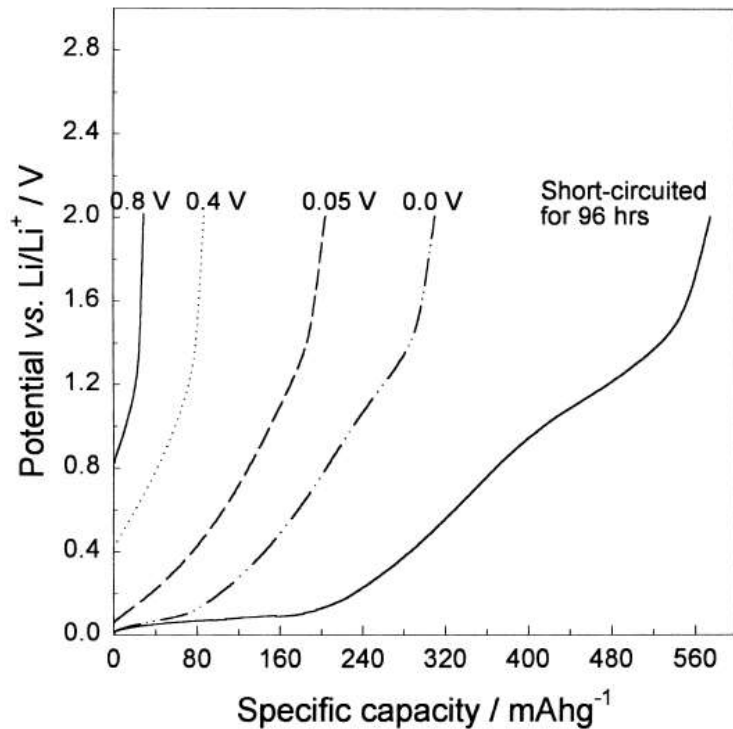


Fig. 5. Galvanostatic discharge curves recorded with the 1000°C material. The charging end is indicated. The experimental conditions were the same as for Fig. 2.

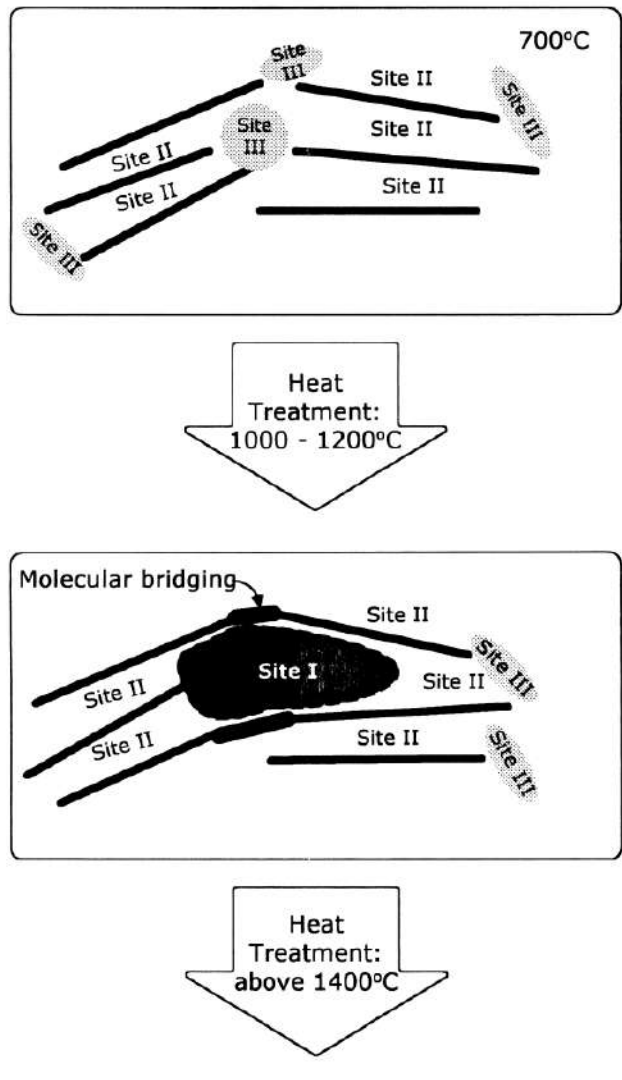


Fig. 7. A schematic illustration for the evolution of site I with heat-treatment temperature.

"Li⁺ storage sites in non-graphitizable carbons prepared from methylnaphthalene-derived isotropic pitches(MNIP)", *Carbon*, 38, 995 - 1001 (2000), C. W. Park, S. I. Lee, S.H. Yoon, S. M. Oh

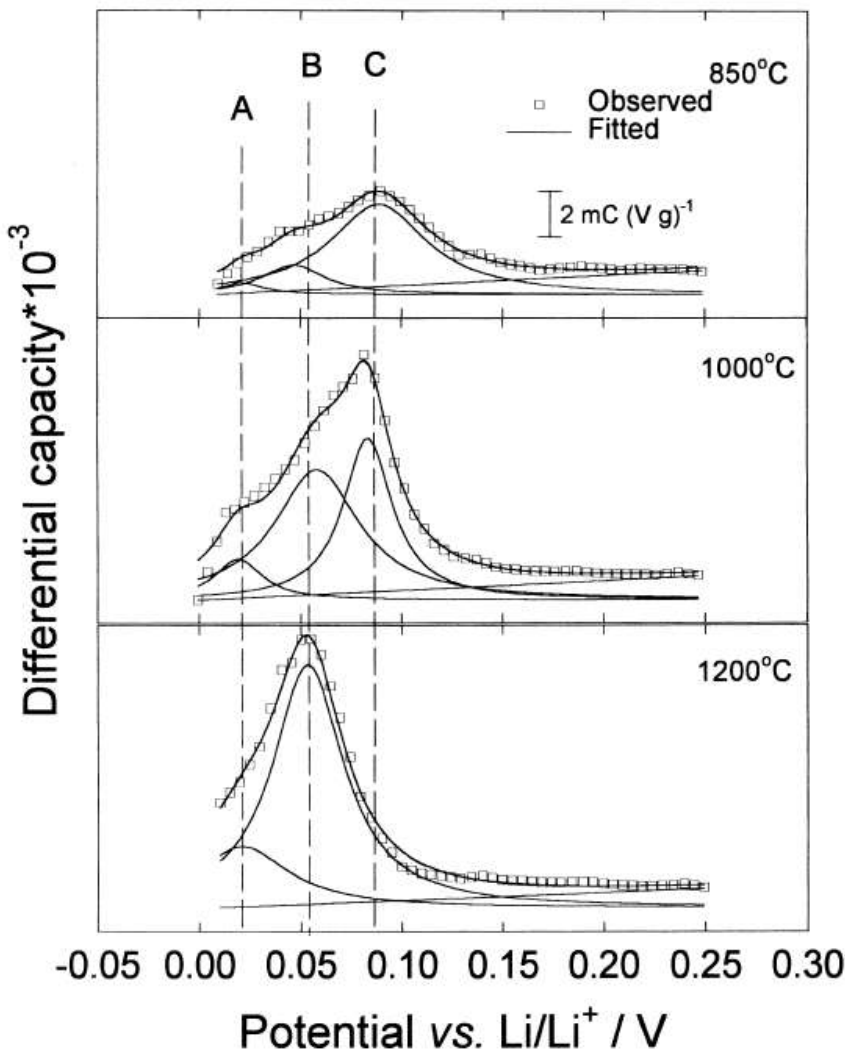
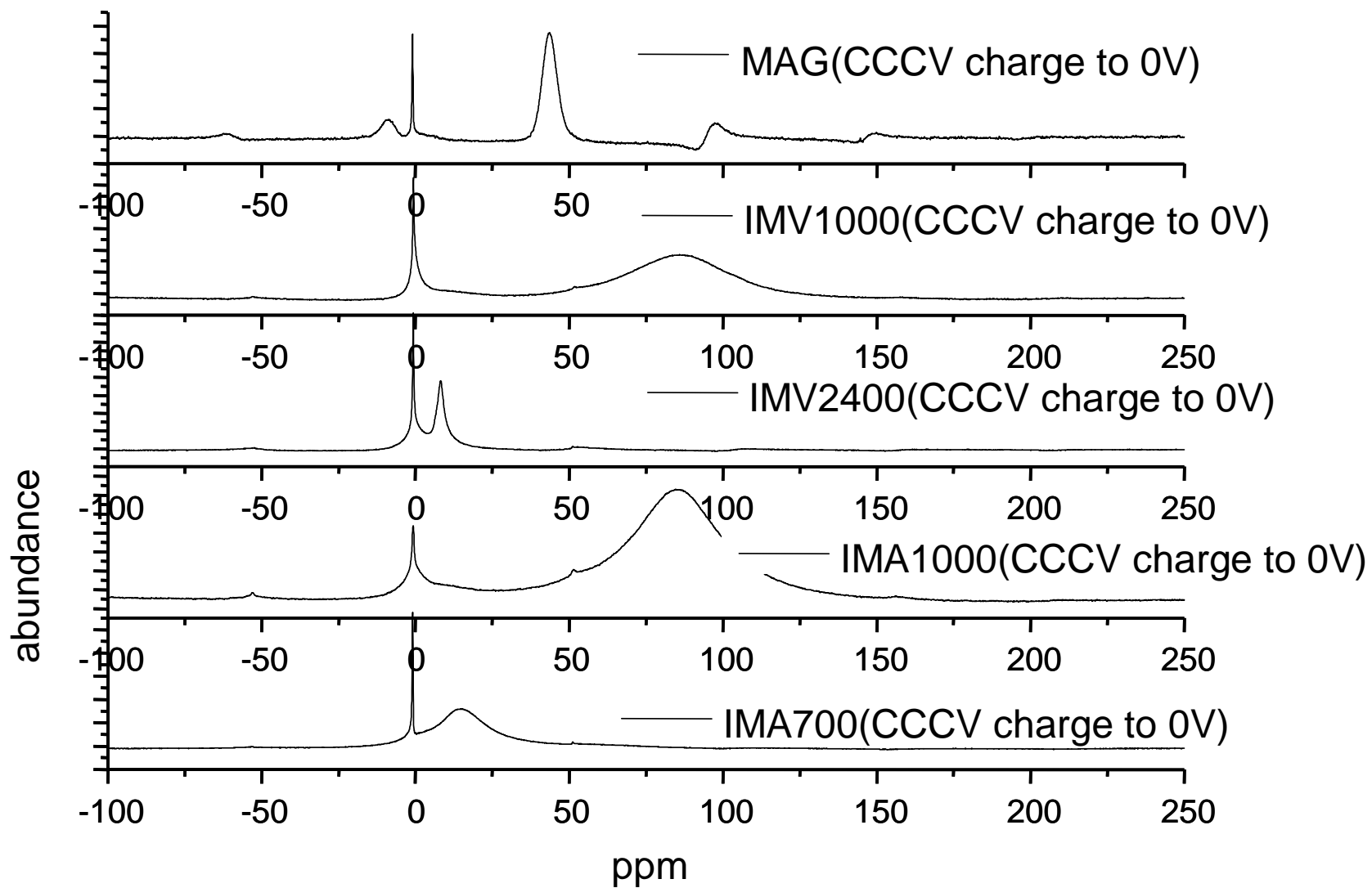
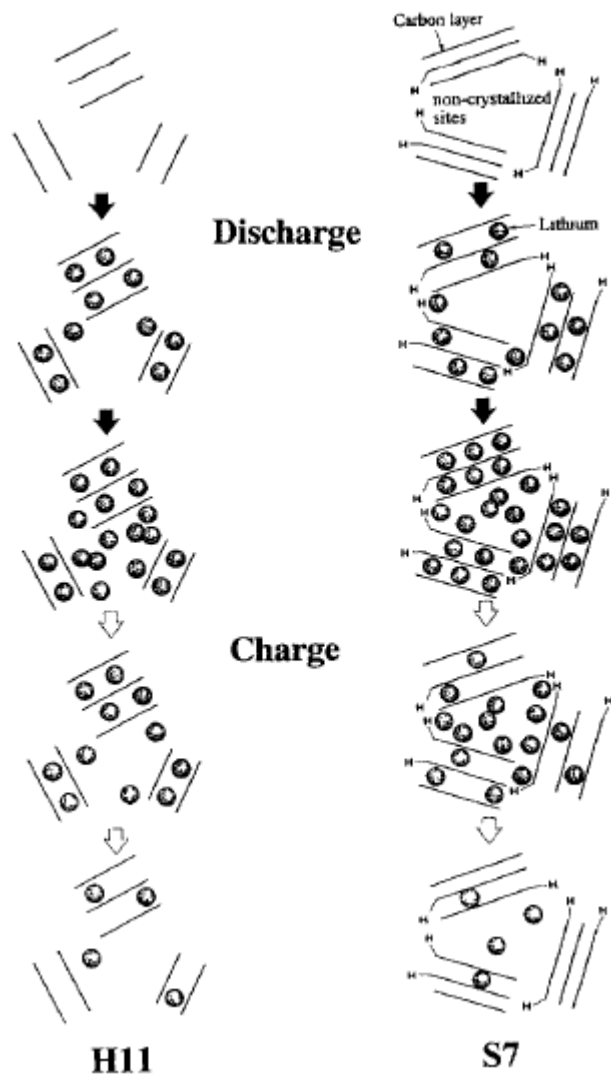


Fig. 8. Expanded view of the discharging EVS profiles near 0 V. The curves were fitted with three Lorentzian peaks. Note the evolution of peaks B and C with the heat treatment temperature.

Li-NMR of Various Carbons



ハードカーボンの充放電機構



Low-crystallized carbon materials for lithium-ion secondary batteries,
Hayato Higuchi, Keiichiro Uenae, Akira Kawakami
JOURNAL OF POWER SOURCES, 68, 1997

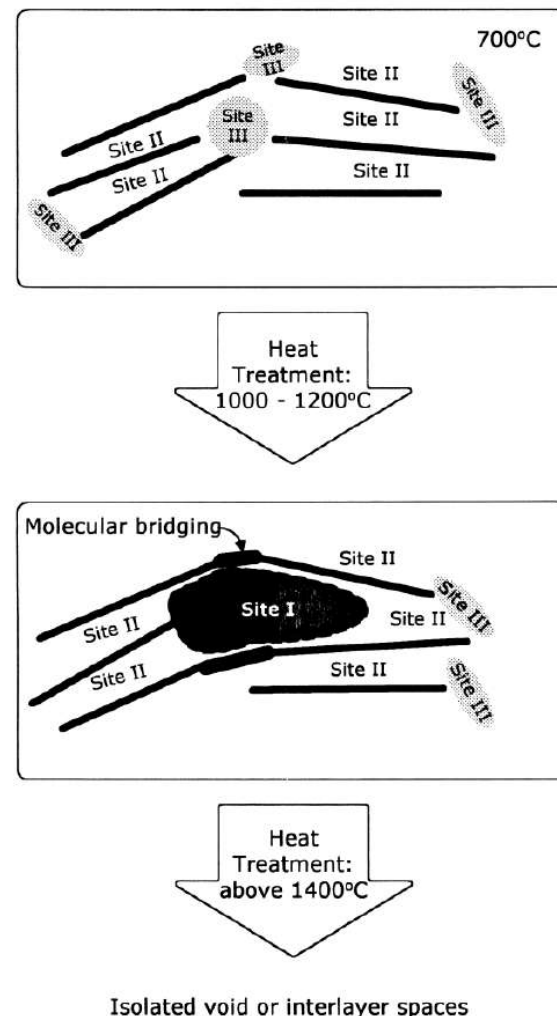
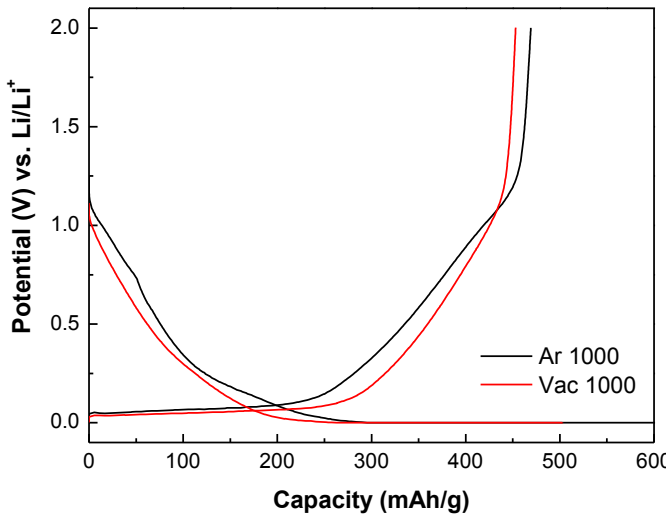


Fig. 7. A schematic illustration for the evolution of site I with heat-treatment temperature.

Hard Carbon from Indonesian Mangrove Char

Ch-Dis Profile



| | Condition | Ch (mAh/g) | Dis (mAh/g) | Efficiency (1cy, %) | Cap.irrev. (mAh/g) |
|----|-----------|---------------|----------------|------------------------|-----------------------|
| IM | Ar 1000 | 628 | 469 | 74.7 | 159 |
| | Vac 1000 | 503 | 453 | 90.1 | 50 |

IM V1000 showed the better initial efficiency than that of IM Ar1000

理想的なハードカーボン

- 高密度: 1.9g/cm³以上
- 高容量: 650mAh/cc
- 高レート性: 90%以上 (5C/0.2C: Half cell, 20C/0.2C:Single cell)
- Low Impurity: 100ppm以下
- 安価: 800円/Kg以下
- 高1st Coulombic efficiency
- 高低温特性
- 高サイクル性
- 豊富な原料からの調製
- マイルドな炭化条件
- Hybrid系が可能な材料: SnO_xまたはSiとのハイブリッド化 ⇒ 高容量化

⇒ 達成するためには、各々因子に対応する原因把握が要求。

⇒ まだ、原因解明が明らかになっていない。

⇒ 今後の研究に期待する。

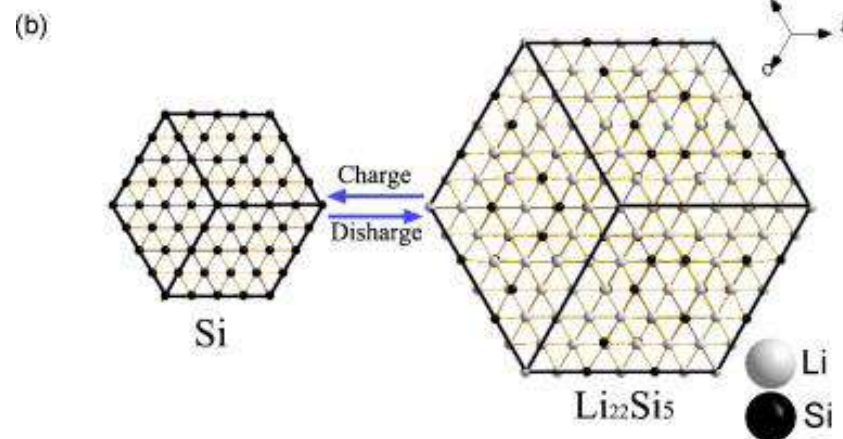
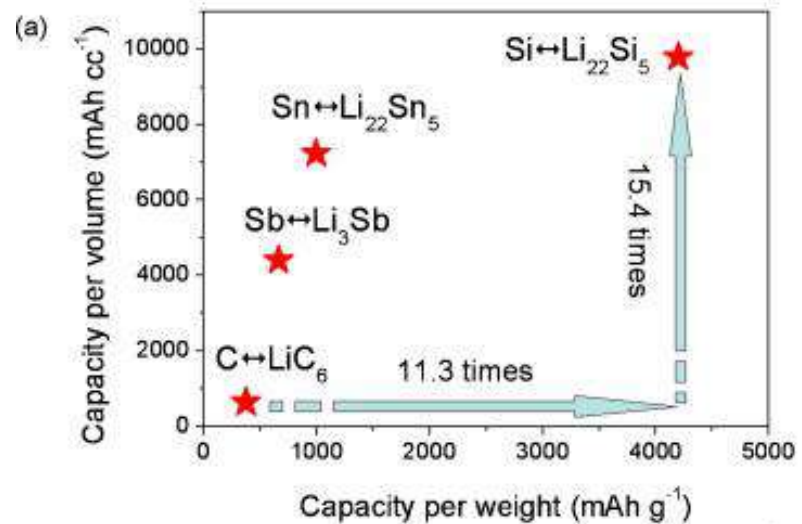


Figure 1-15. Typical high performance materials as anode ;
 (a) Comparison of graphite, Si, Sn and Sb
 (b) Volume expansion model of Si during charge

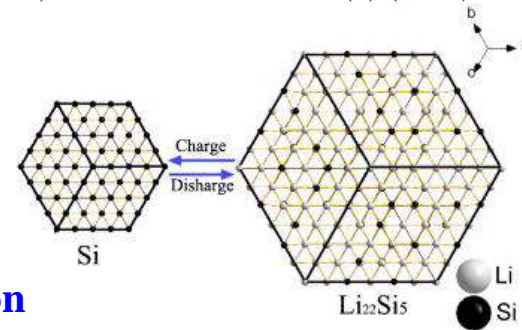
High performance material & their problems

- **SiO, Si and Sn** (SiO 2100, Si 4200, Sn 931 mAh/g) are very promising materials as anodic materials of LIB for their large theoretical capacities, however, they have poor cycle performances because of internal crack in particles caused by large volumetric expansion in charge process.

Li-Si system

| Compound | Structure | Unit cell vol. (\AA^3) | Vol. / Si atom (\AA^3) |
|-----------------------------|--------------|--------------------------------------|--------------------------------------|
| Si | Cubic | 160.2 | 20.0 |
| $\text{Li}_{12}\text{Si}_7$ | Orthorhombic | 243.6 | 58.0 |
| $\text{Li}_{14}\text{Si}_6$ | Rhombohedral | 308.9 | 51.5 |
| $\text{Li}_{13}\text{Si}_4$ | Orthorhombic | 538.4 | 67.3 |
| $\text{Li}_{22}\text{Si}_5$ | Cubic | 659.2 | 82.4 |

Ref.) J. Power Sources 192 (2) (2009) 644-651



Ref. : A. John Appleby and et al., J Power Sources 163 (2007) 1003-1039

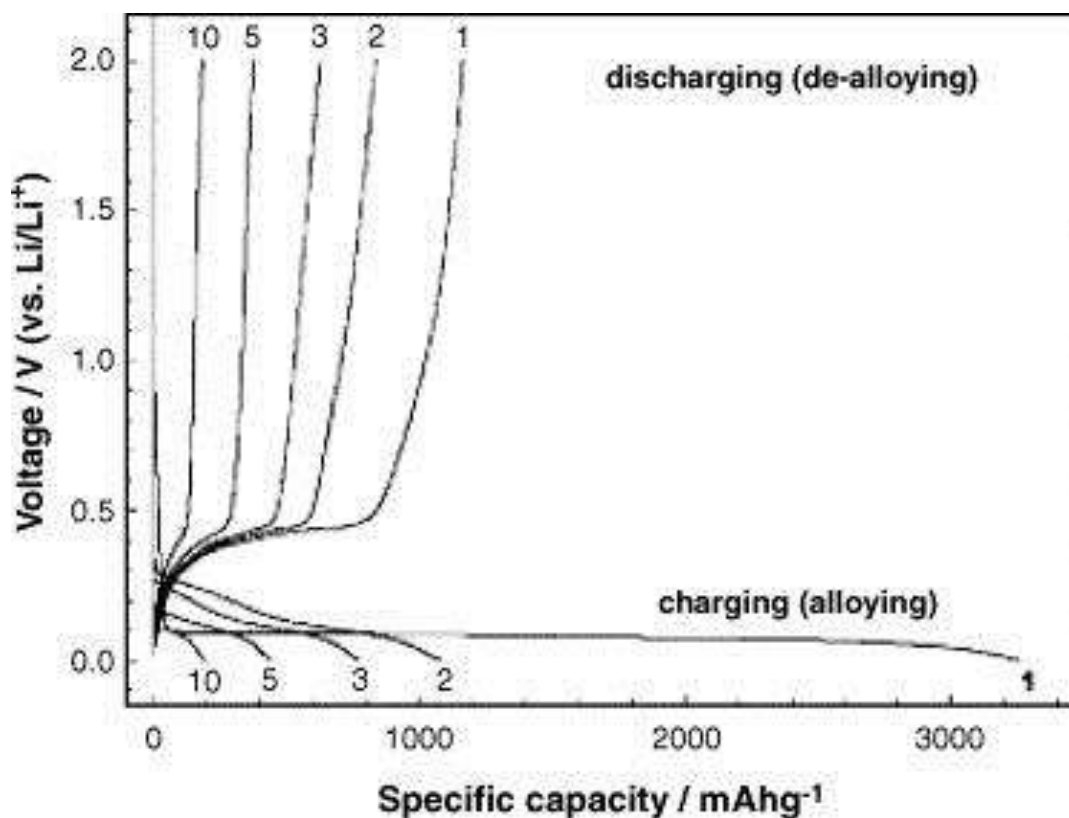
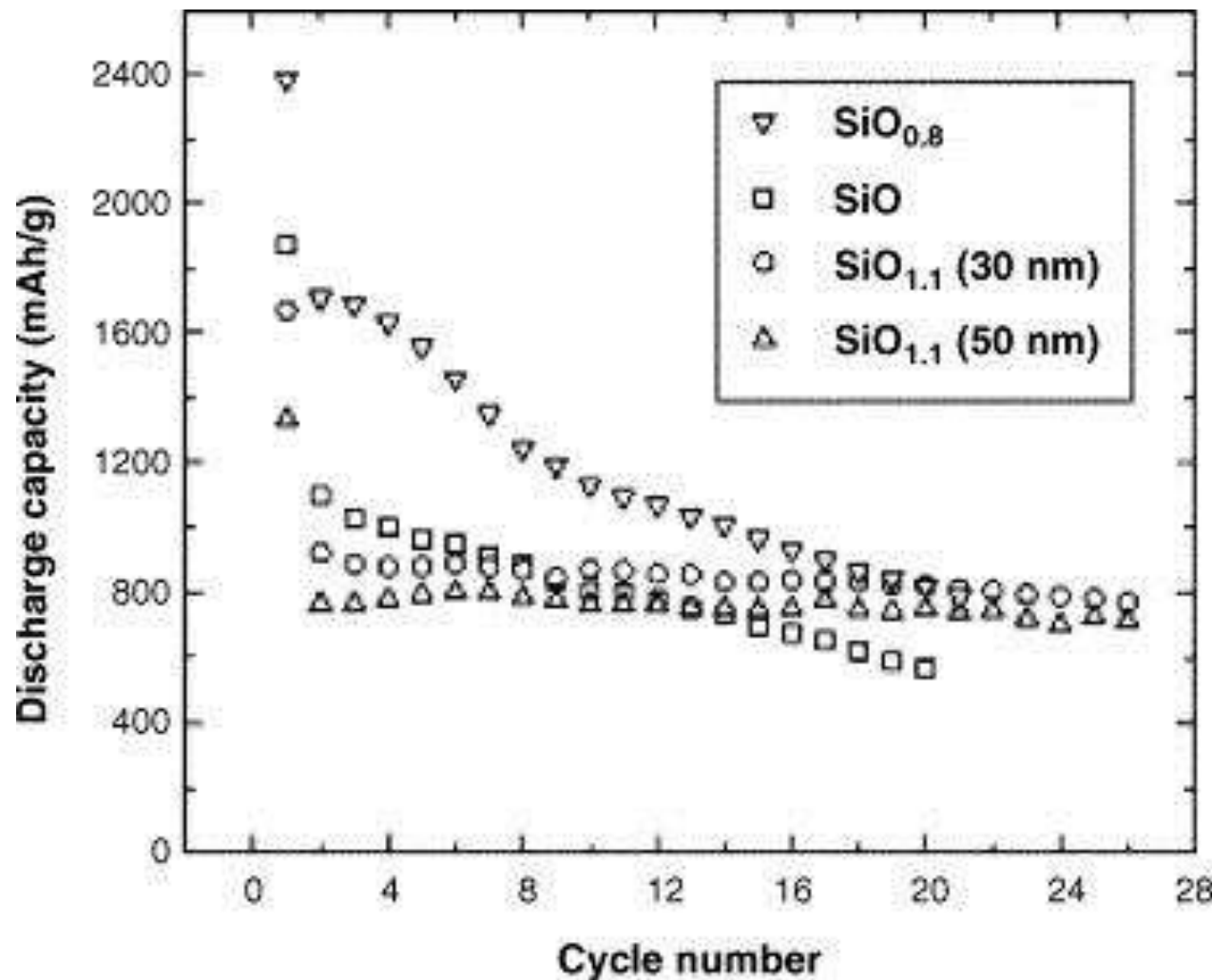


Fig. 2. Galvanostatic charge–discharge profiles for micro-Si (10 μm) anode.

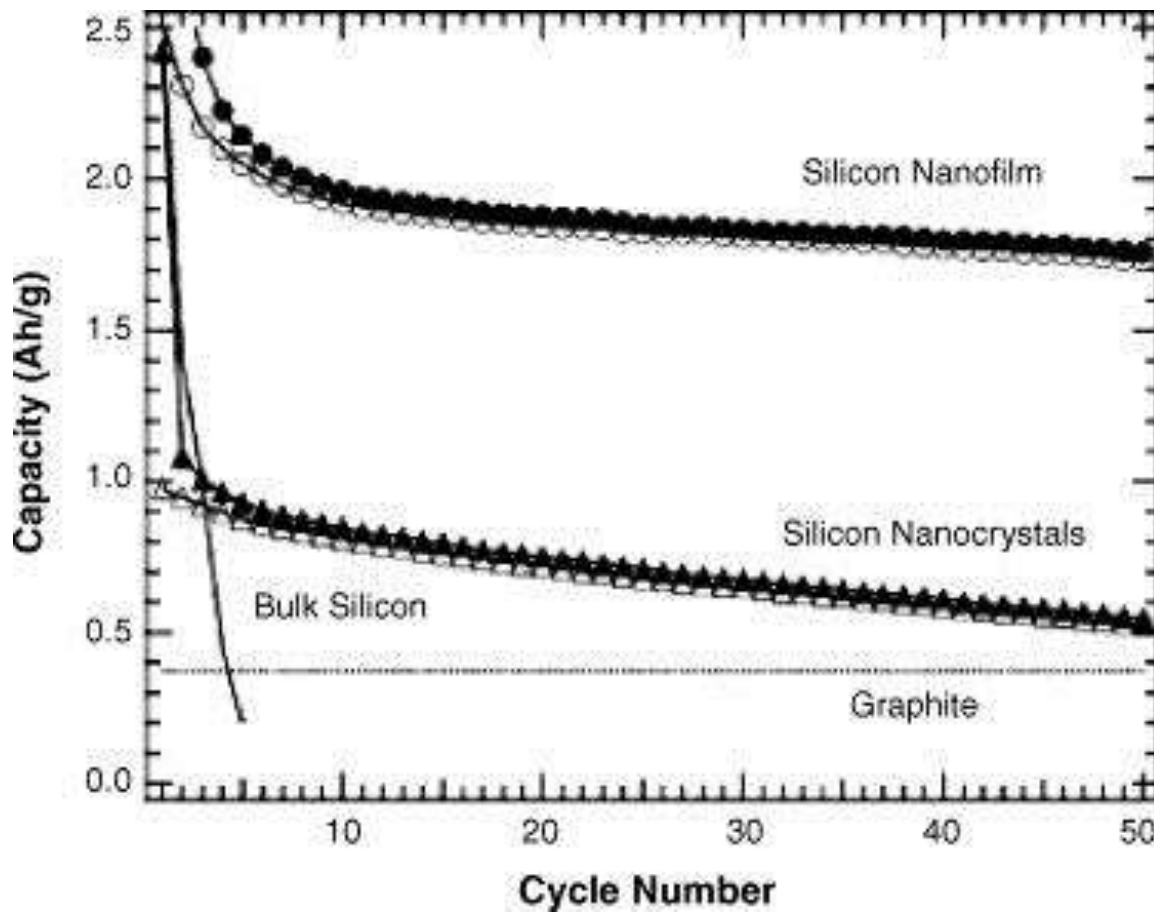
J.H. Ryu, J.W. Kim, Y.-E. Sung, S.M. Oh

Electrochem. Solid State Lett., 7 (2004), p.
A306



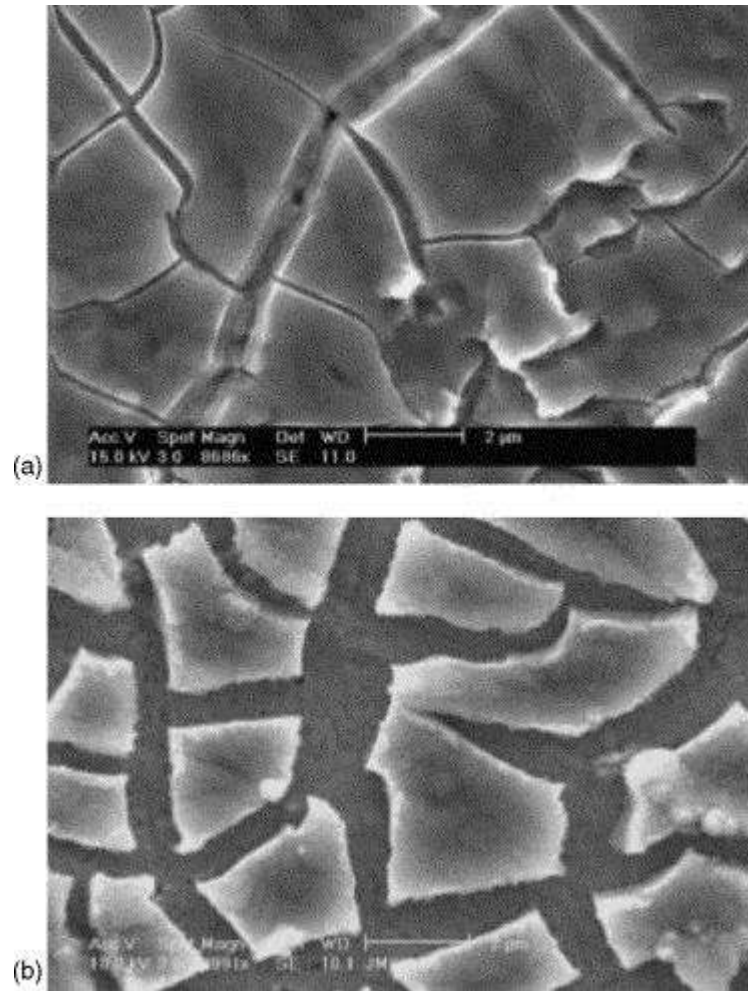
Cycling behavior of SiO_x with different oxygen content and particle size

J. Yang, Y. Takeda, N. Imanishi, C. Capiglia, J.Y. Xie, O. Yamamoto
Solid State Ionics, 152–153 (2002), p. 125



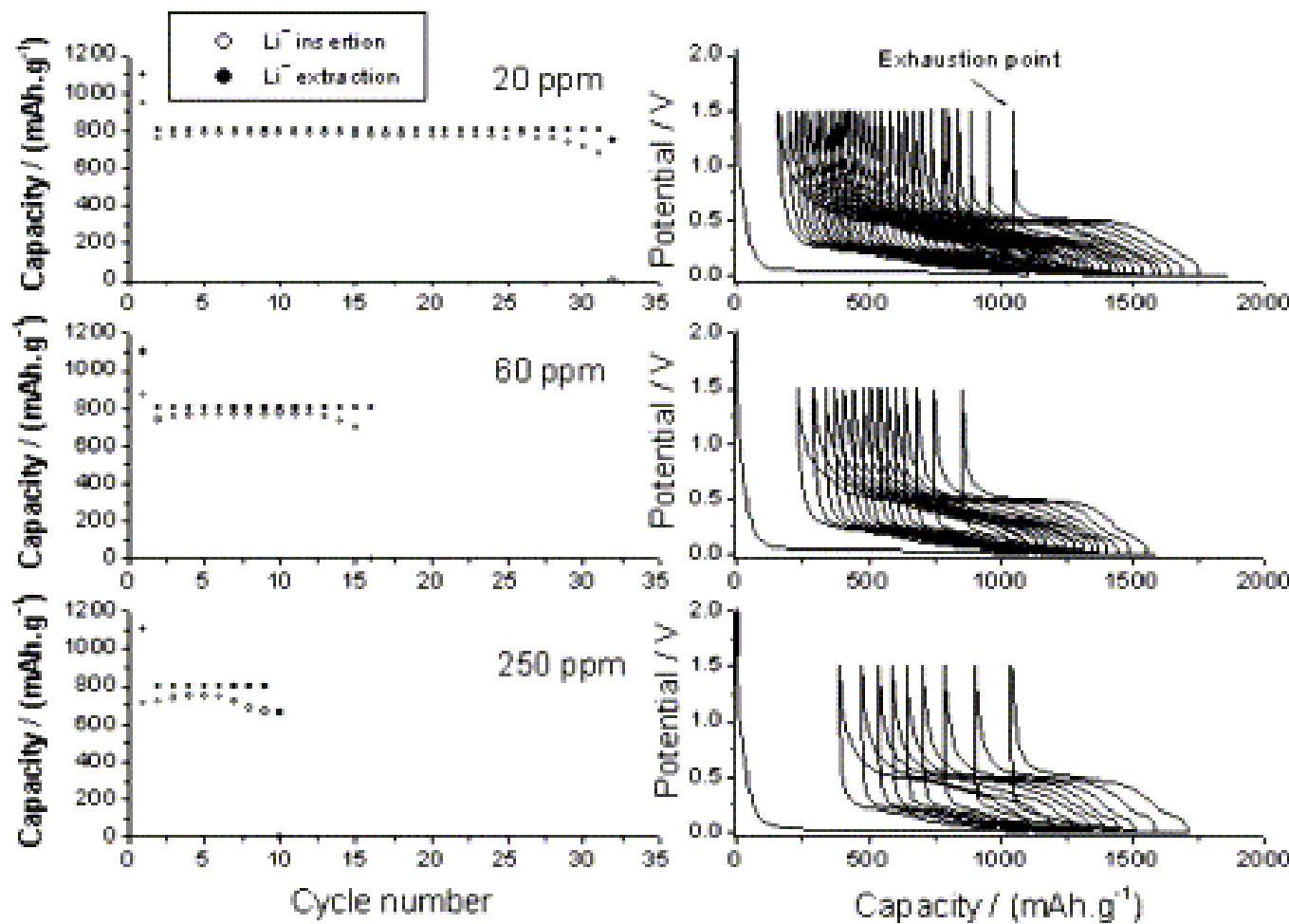
Specific capacity vs. cycle number for nano-crystalline Si and nano-amorphous Si thin film anodes prepared by thermal vapor deposition. Specific capacity of graphite and bulk-silicon anodes also shown

J. Graetz, C.C. Ahn, R. Yazami, B. Fultz
Electrochem. Solid-State Lett., 6 (2003), p. A194



SEM morphology of 250 nm a-Si film on Cu cycled at C/2.5 for (a) 1 cycle, and (b) 30 cycles

J.P. Maranchi, A.F. Hepp, A.G. Evans, N.T. Nuhfer, P.N. Kumta
J. Electrochem. Soc., 153 (2006), p. A1246



Cycling performance of carbon-coated silicon anodes in 1 M LiPF₆ EC:DMC (1:2) at different water contents present in the electrolyte. In all cases, the 'exhaustion point' (last extraction peak) is centered around 1000 mA h/g

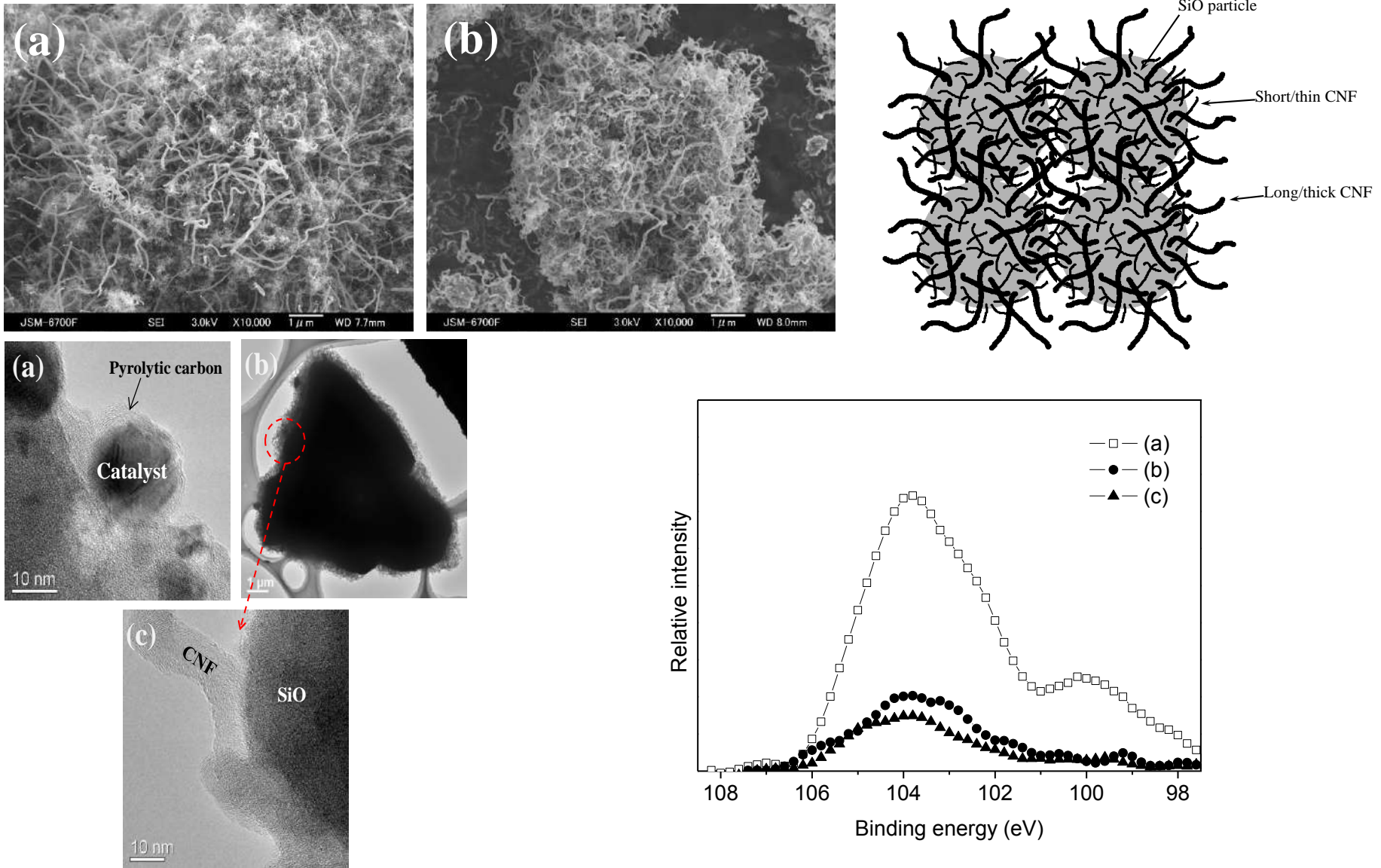


Figure Schematic model of cocoon shaped composite of silicon monoxide and surficial carbon nanofiber (SiO-CNF composite)

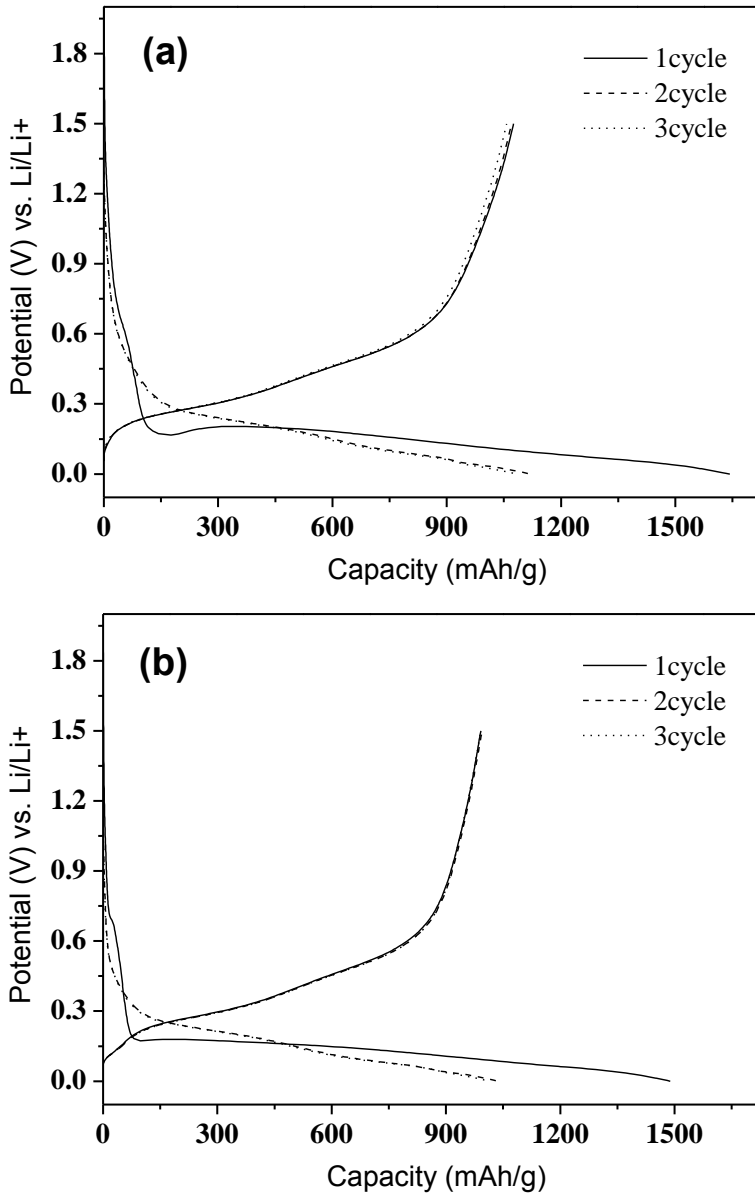
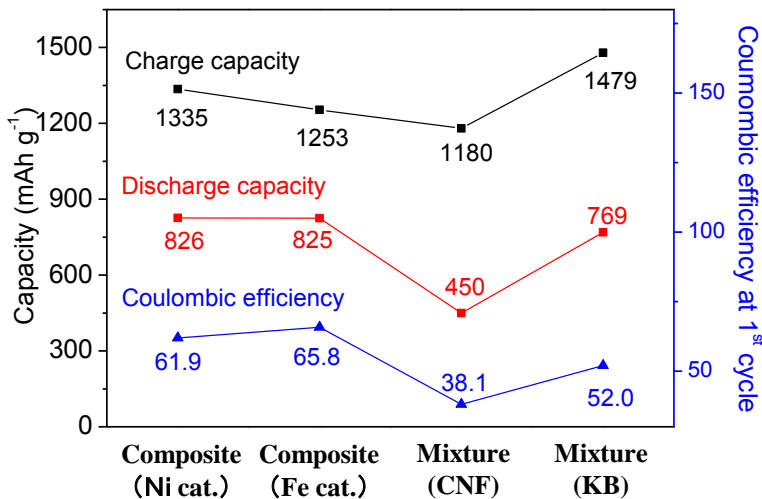


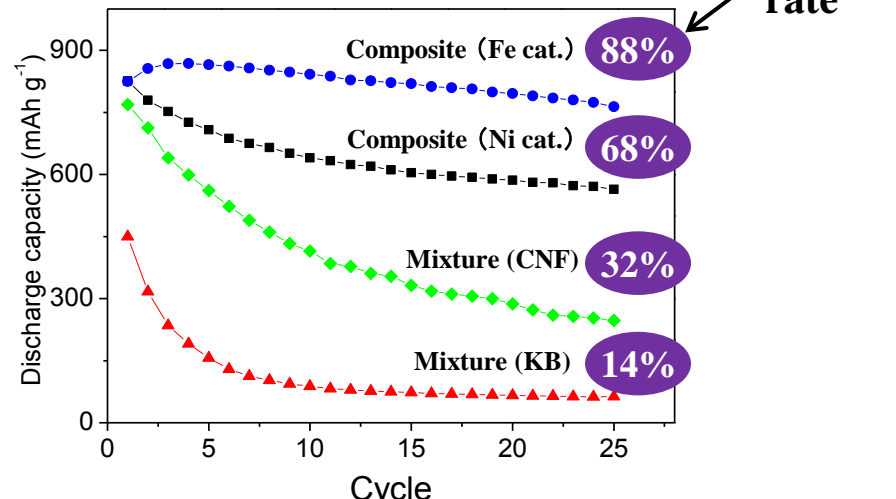
Figure Cycle performances with SiO-CNF composite until 3 cycles according to the various amount of CNFs with Ni (a) or Fe catalyst (b).

Comparison bet. Composite and Mixture

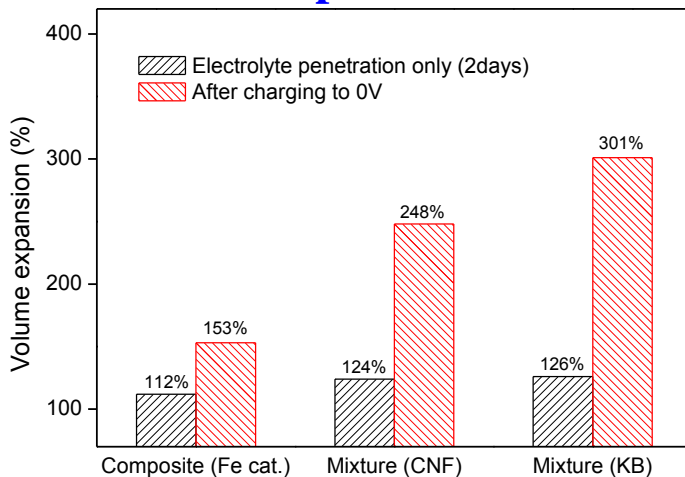
At 1st cycle



Cycle performance



Volume expansion



Superiority of the CNF composite

- High discharge capacity and coulombic efficiency at 1st cycle
 - Excellent cycle performance
 - Lower volume expansion
- ⇒ CNF growth provides spaces to relieve volume expansion and conductivities to improve performances

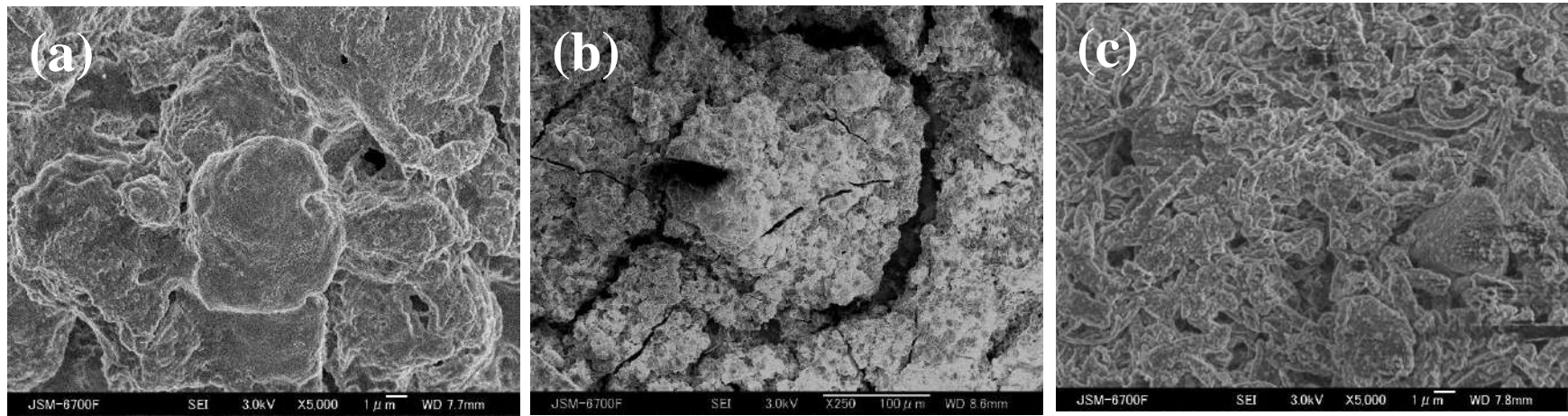
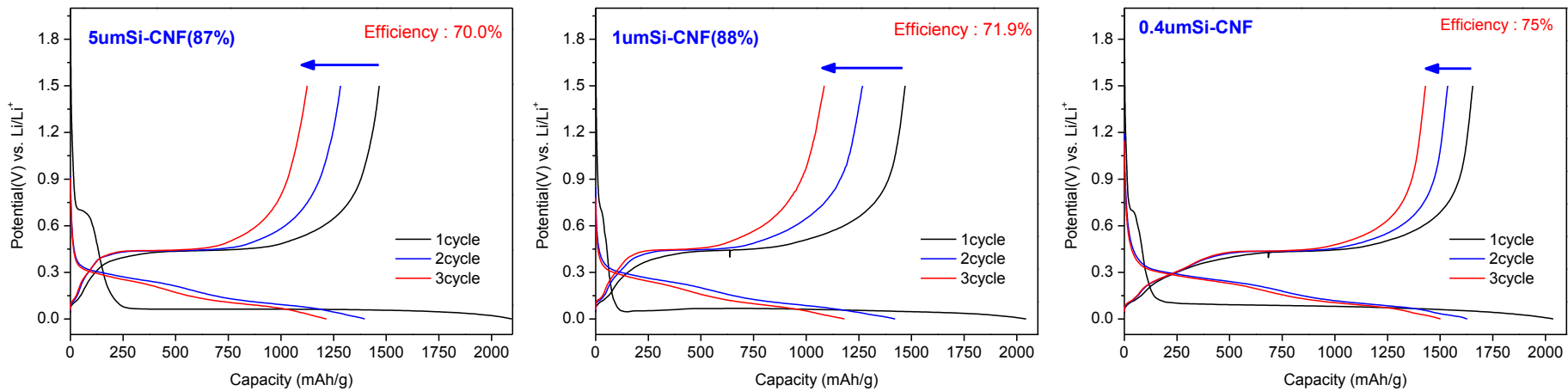


Figure 2-12. SEM images of electrode surface after 3 cycles : (a) SiO-CNF composite with Fe catalyst, mixture of SiO-KB (b) or SiO-CNF (c).

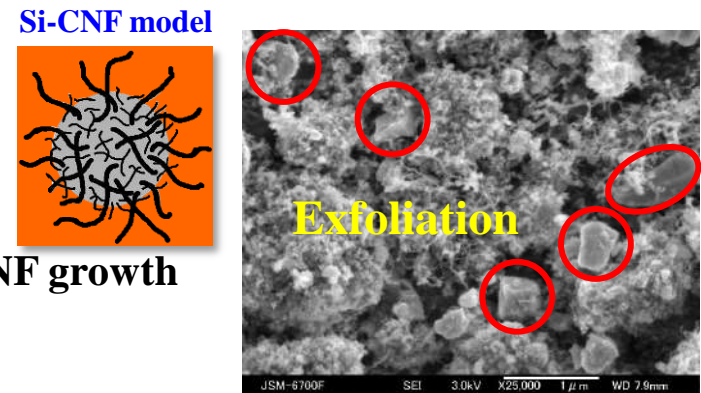
Problem in Si-CNF composite

Si-CNF composite : CNF growth directly on Si(5um, 1um, 0.4um)



Problems of Si-CNF composite

- Small particle size, under 1um, is reasonable
- Poor initial efficiency because of high surface area by CNF growth
- Binding force bet. Si and CNF are needed
- Although CNF growth on Si particle of 0.4um (Si-CNF composite), Si-CNF composite didn't show improved cycle performance because CNF exfoliated from Si which had **no surface acidity**.

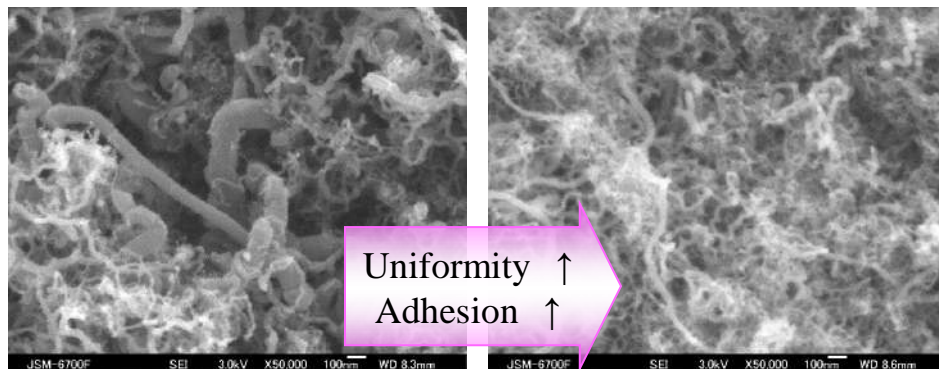
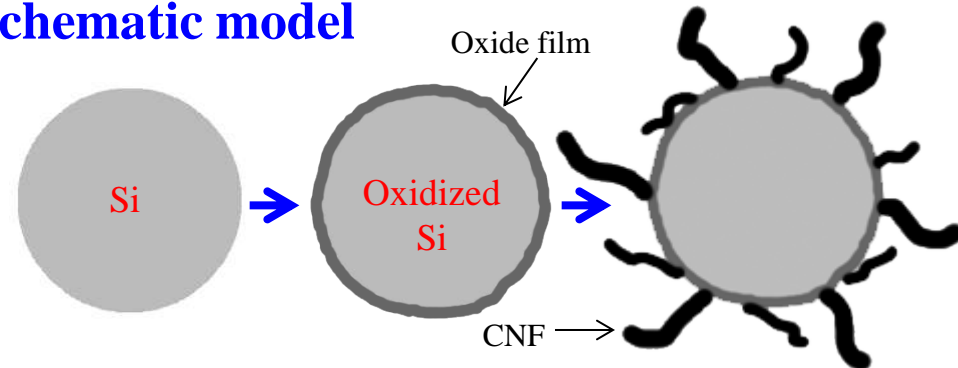


Oxidized Si-CNF composite

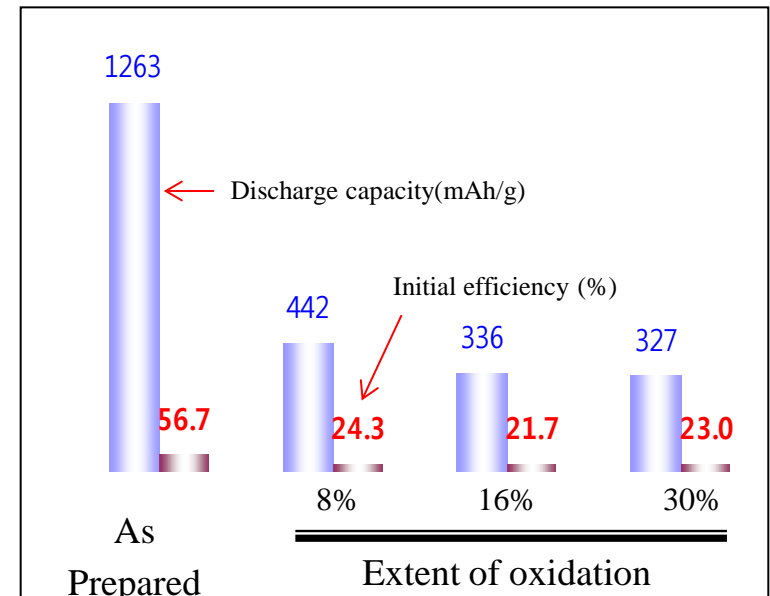
To improve surface acidity,

Si particle was oxidized at 700~900°C for 3 hrs with H₂O_g.

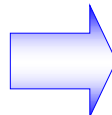
Schematic model



Performance test



Adhesive power and uniformity of CNF was improved by surface oxidized Si, whereas charge-discharge performance became poor.

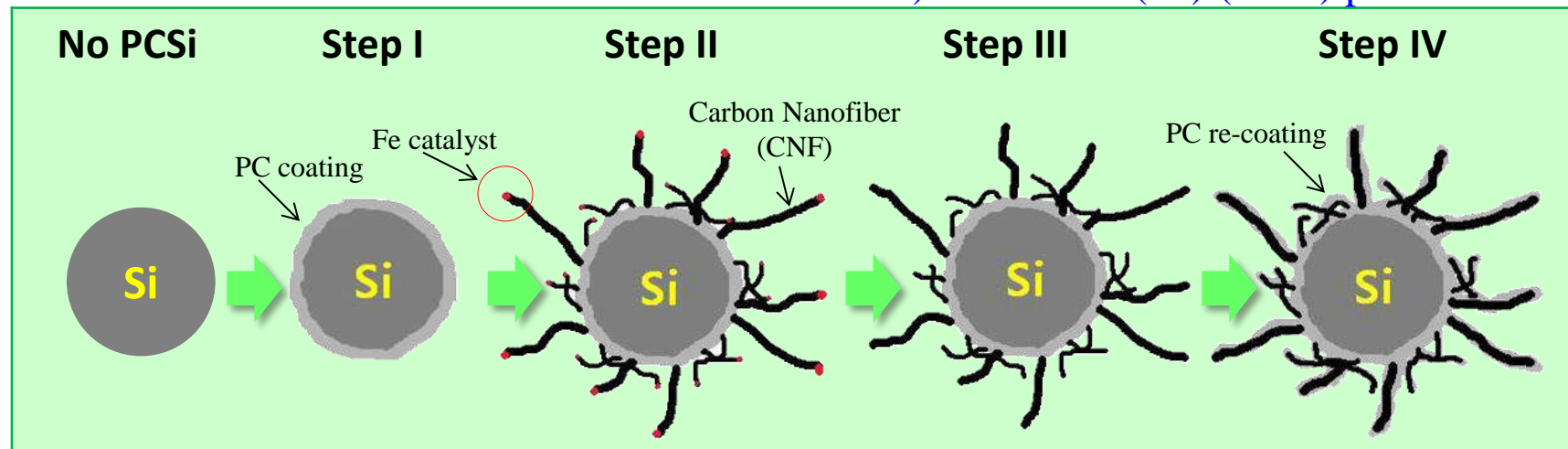


Composite of PC coated Si and CNF

As a solution, Pyrolytic carbon (PC) coating on Si particle is suggested.

- **Step I :** PC is coated on Si particle to improve adhesion between Si and CNF (PCSi).
⇒ The coated PC provide conductivity with Si particles as well as adhesion strength.
- **Step II :** CNF is grown on PCSi to improve cycle performance
- **Step III :** Removal catalyst by HCl treatment
- **Step IV :** PC is re-coated on PCSi-CNF composite to improve initial efficiency by decreasing surface area.

Ref.) Carbon 47 (15) (2009) p.3338-3391

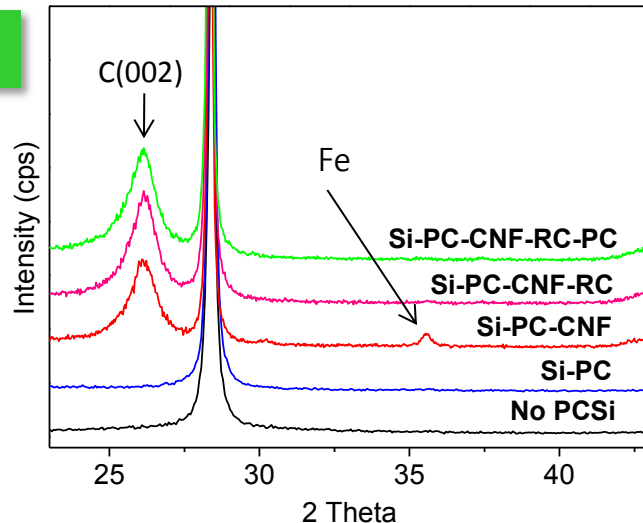


Preparation of PCSi-CNF composite

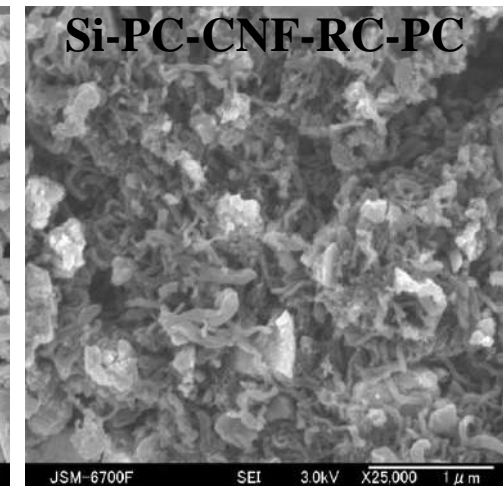
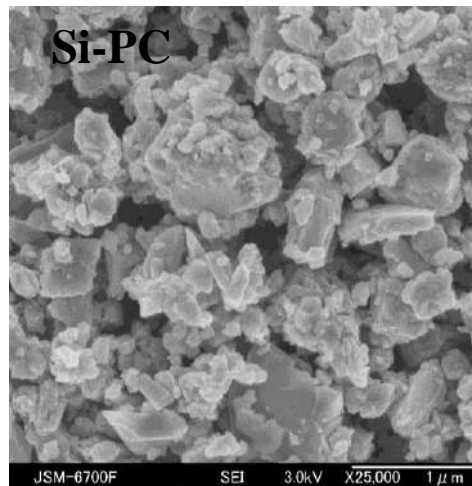
| | Code | PC/ or CNF amount (wt. %) | | | Condition |
|------------|----------------------------|---------------------------|------|---------------|---|
| | | PC | CNF | PC re-coating | |
| Samples | Step I Si-PC | 6 % | - | - | PC coating (900°C-CH ₄ /He- 30min) |
| | Step II Si-PC-CNF | 6 % | 93 % | - | CNF growth on PCSi (580°C-CO/He- 30min) |
| | Step III Si-PC-CNF-RC | 6 % | 93 % | - | Catalyst removal by HCl |
| | Step IV Si-PC-CNF-RC-PC | 6 % | 93 % | 8 % | PC re-coating (900°C-CH ₄ /He- 30min) |
| Comparison | Si-CNF | - | 98 % | - | CNF growth directly on Si surface |

Analysis of PCSi-CNF composite

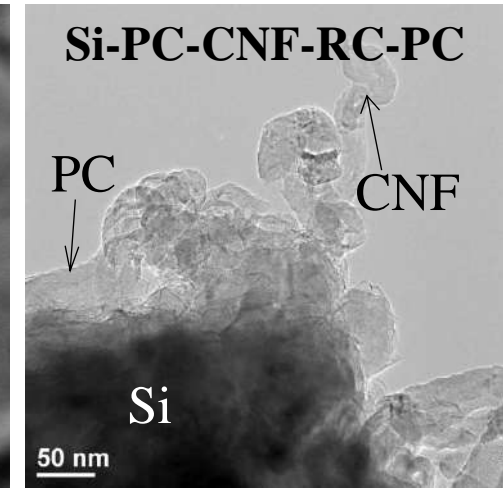
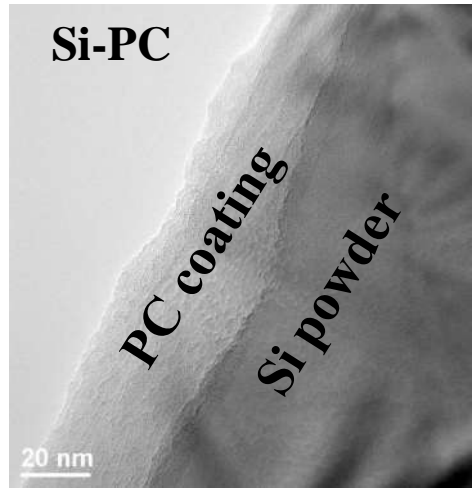
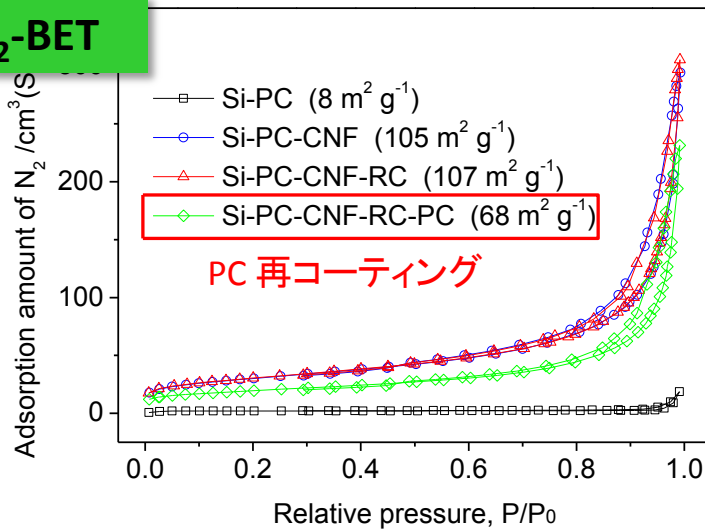
XRD



SEM & TEM

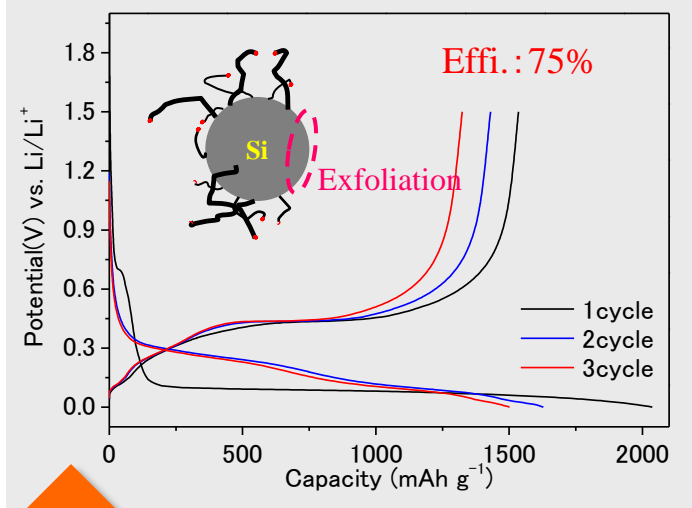


N₂-BET

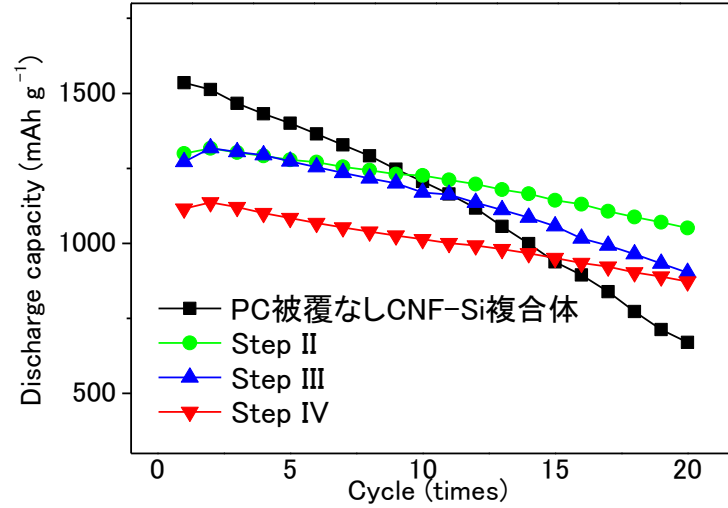


Cycle performances of PCSi-CNF composite

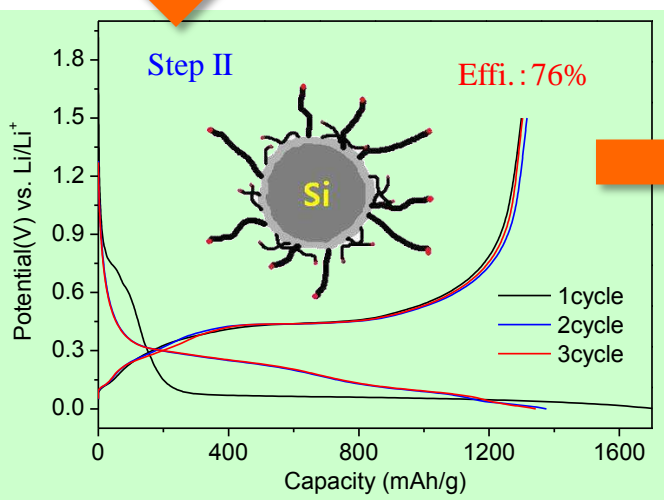
Si-CNF composite



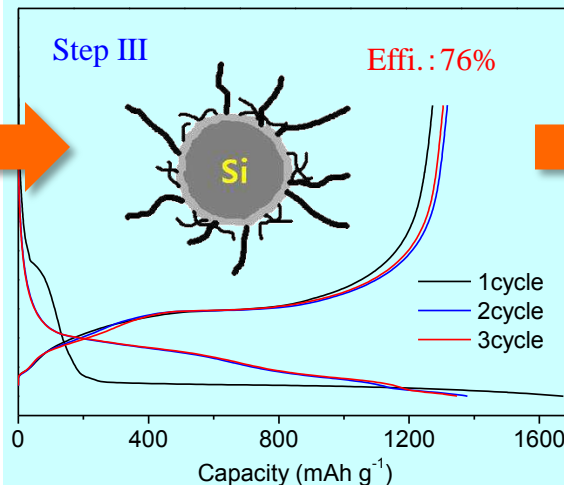
Cycle performance



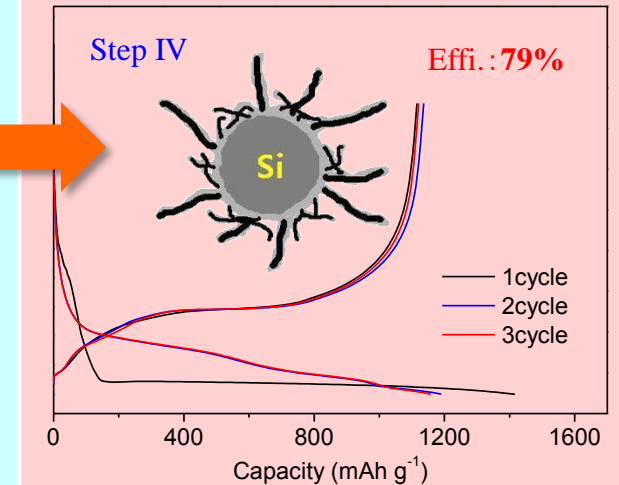
↑
↓
PCSi-CNF



PCSi -CNF (Fe removal)



PCSi -CNF (PC re-coating)



The decreased surface area

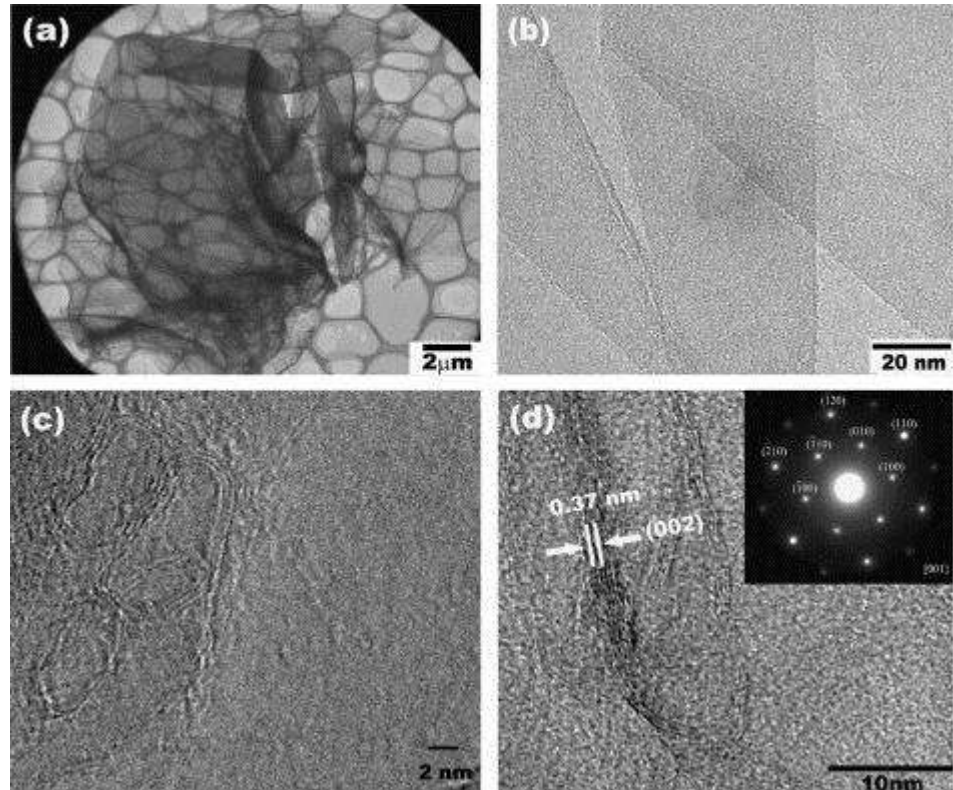
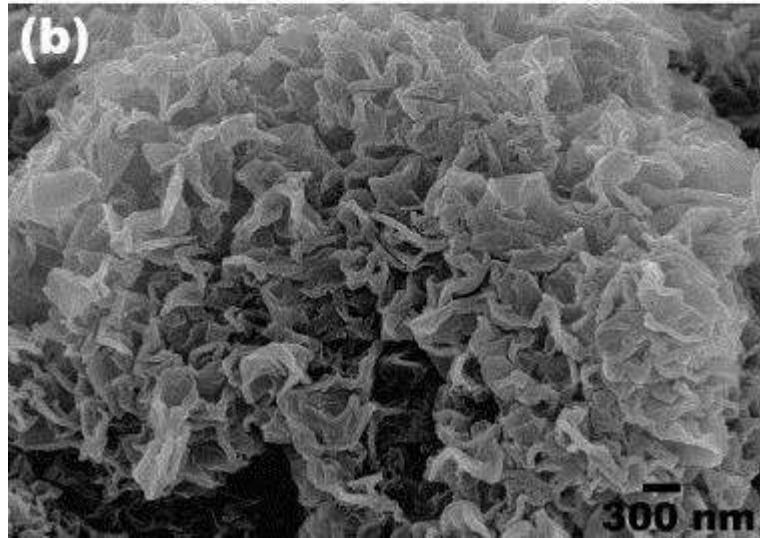
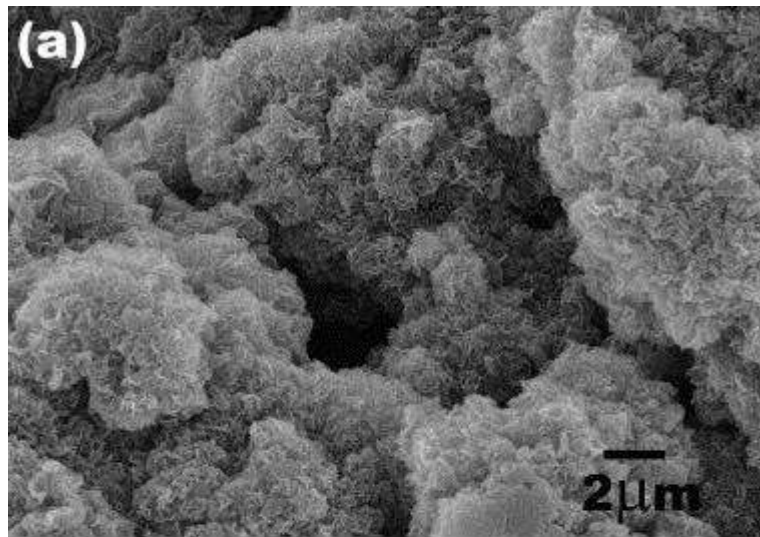
Cycle performances of PCSi-CNF composite

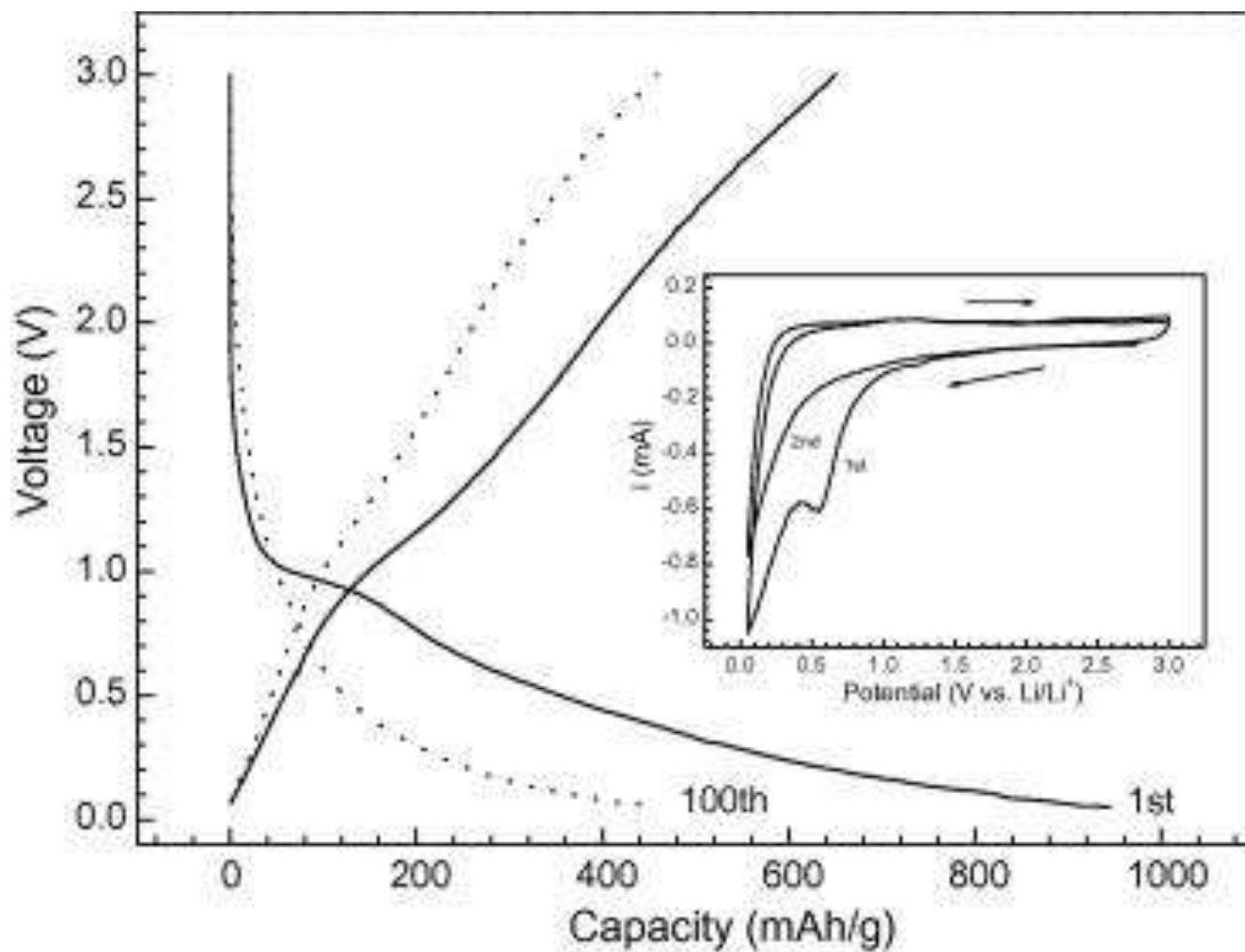
| | | Capacity at 1 st cycle (mAh/g) | | |
|------------|-----------------|---|------|-------|
| | | Ch | Dis | 效率(%) |
| Samples | Si-PC-CNF | 1709 | 1299 | 76.0 |
| | Si-PC-CNF-RC | 1674 | 1272 | 76.0 |
| | Si-PC-CNF-RC-PC | 1415 | 1115 | 78.8 |
| Comparison | Si-CNF | 2037 | 1535 | 75.4 |

| | | Dis.(max) (mAh /g) | At 20 cycle (mAh/ g) | |
|------------|-----------------|-----------------------|----------------------|--------------------|
| | | | Dis | Retention rate (%) |
| Samples | Si-PC-CNF | 1317 | 1051 | 80 |
| | Si-PC-CNF-RC | 1318 | 903 | 69 |
| | Si-PC-CNF-RC-PC | 1136 | 873 | 77 |
| Comparison | Si-CNF | 1535 | 670 | 44 |

Graphene nanosheets for enhanced lithium storage in lithium ion batteries

[Carbon, 47, 2009, 2049–2053, G. Wang et al.](#)



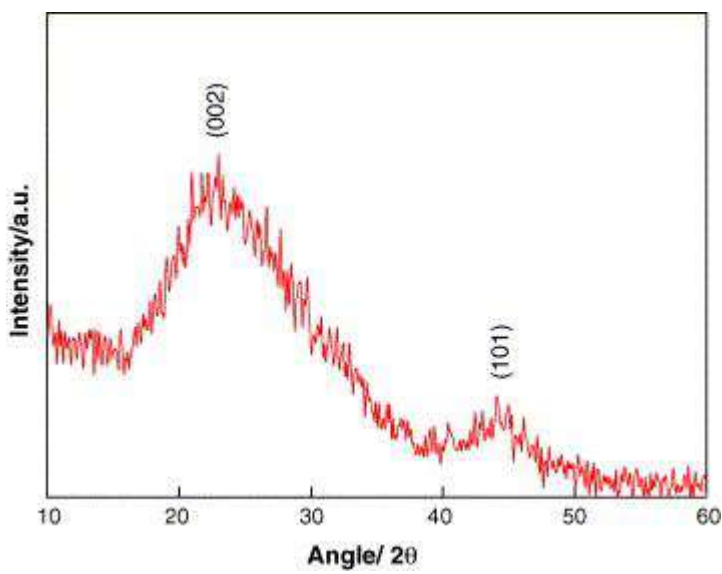
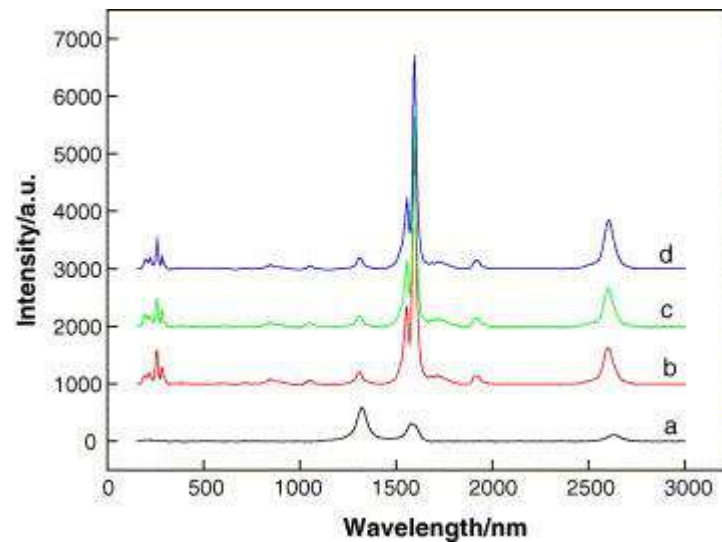
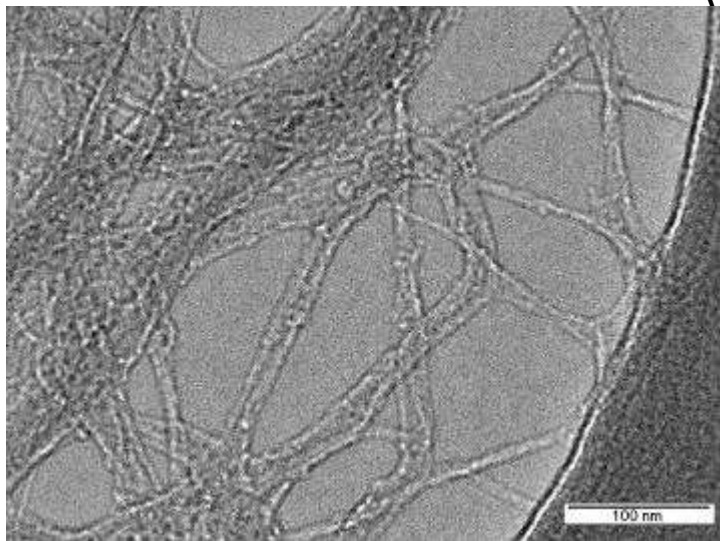


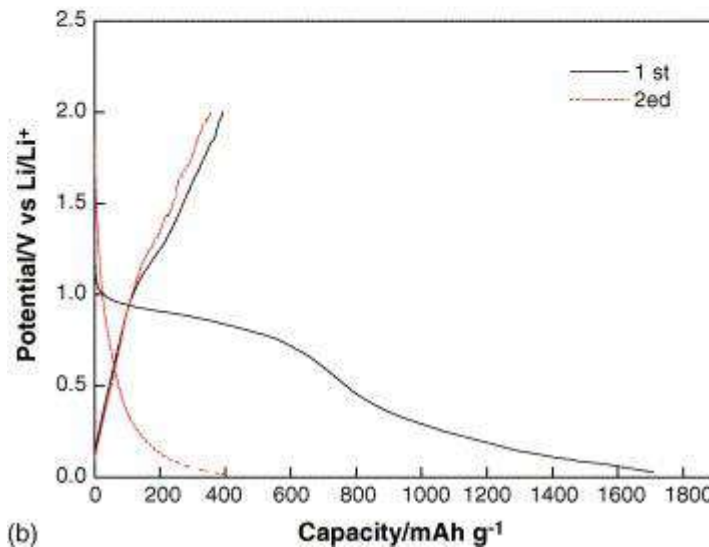
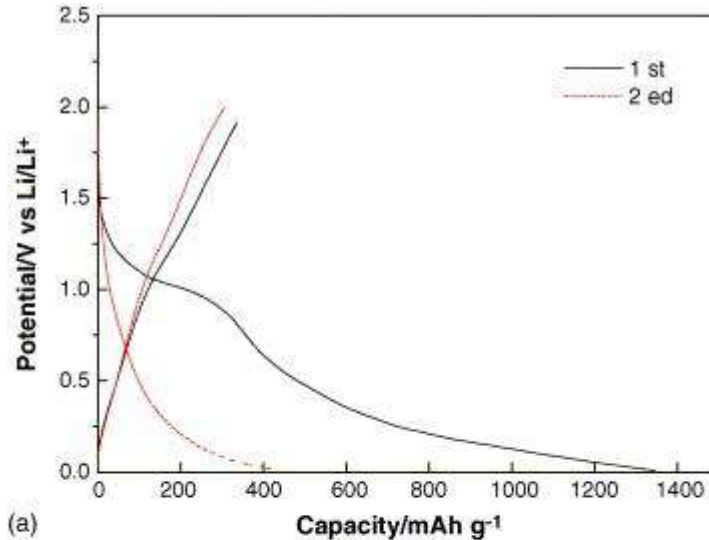
Charge and discharge curves of graphene nanosheets as anode in lithium-ion cells. The inset is the cyclic voltammograms of graphene nanosheet electrode

Single wall carbon nanotube paper as anode for lithium-ion battery

Electrochimica Acta

Volume 51, Issue 1, 5 October 2005, Pages 23–28



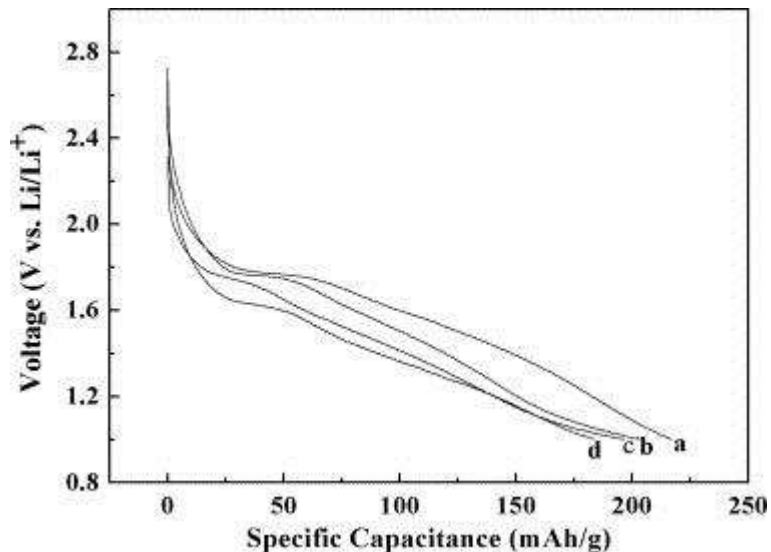
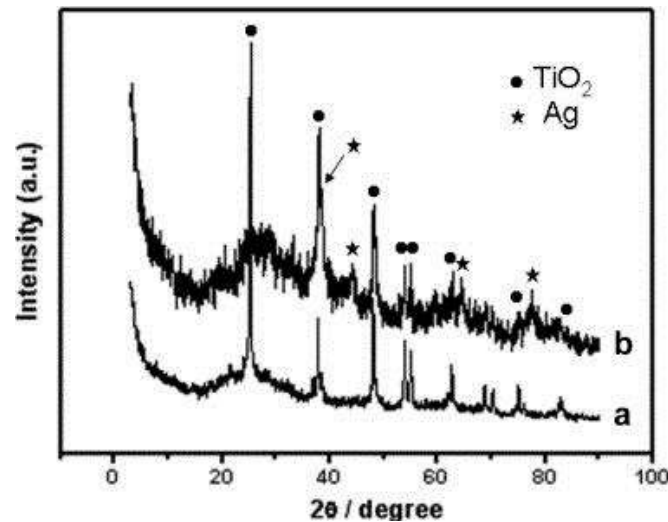
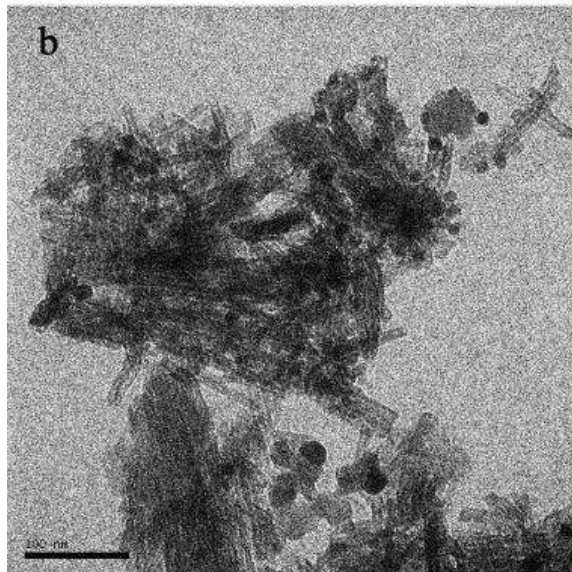
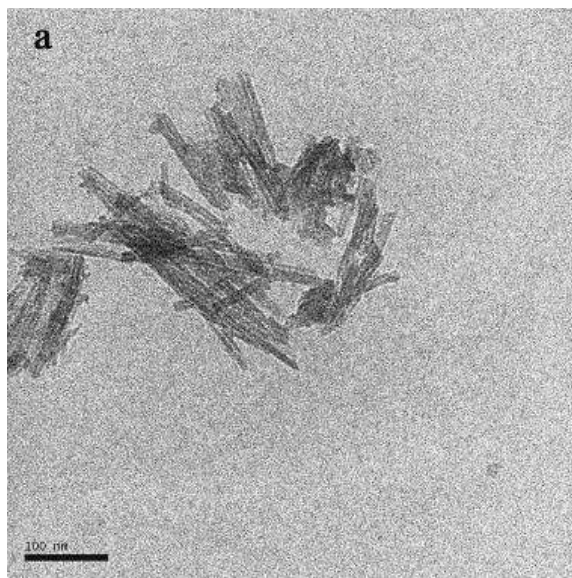


The charge/discharge profiles of SWNT electrodes: (a) conventional slurry coated electrode and (b) "Free standing" electrode.

Preparation and electrochemical properties of Ag-modified TiO₂ nanotube anode material for lithium–ion battery

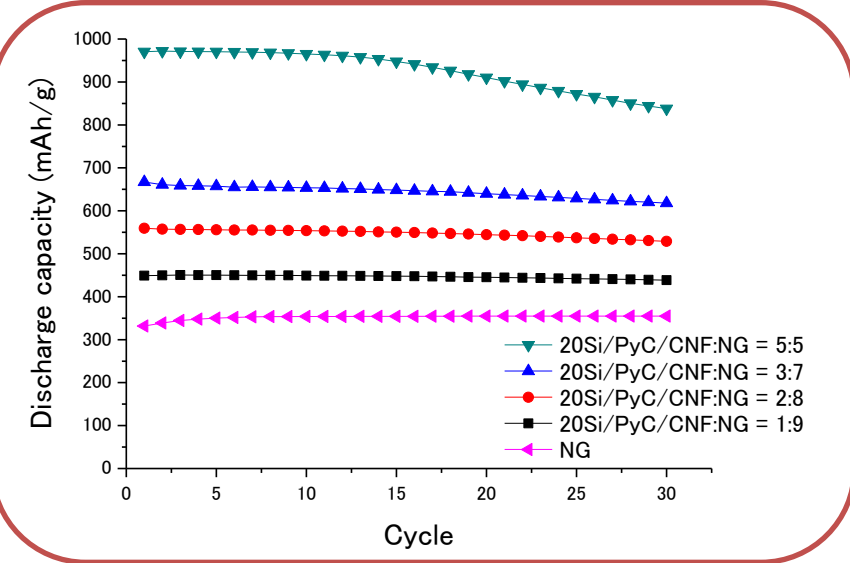
[Electrochemistry Communications](#)

[Volume 9, Issue 3, March 2007, Pages 425–430](#)

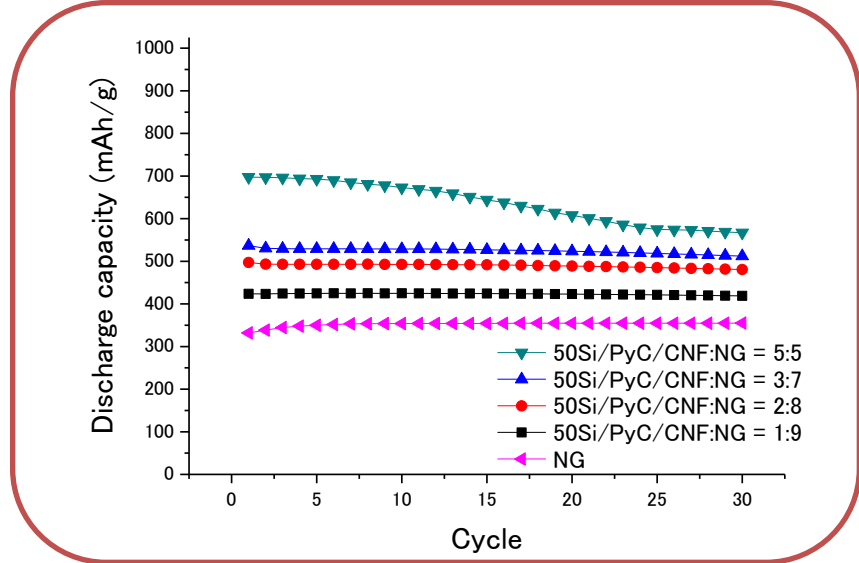


Hybridization of Si/PyC/CNF and NG

20Si/PyC/CNF and NG



50Si/PyC/CNF and NG



| Sample | 1 st cycle Coulombic efficiency (%) | Retention ratio (% , 30 th /1 st) |
|---------------------|--|--|
| 20Si/PyC/CNF:NG=5:5 | 63.6 | 86.3 |
| 20Si/PyC/CNF:NG=3:7 | 67.5 | 92.6 |
| 20Si/PyC/CNF:NG=2:8 | 74.2 | 94.5 |
| 20Si/PyC/CNF:NG=1:9 | 80.3 | 97.7 |
| NG | 90.0 | 106.9 |

| Sample | 1 st cycle Coulombic efficiency (%) | Retention ratio (% , 30 th /1 st) |
|---------------------|--|--|
| 50Si/PyC/CNF:NG=5:5 | 63.1 | 81.4 |
| 50Si/PyC/CNF:NG=3:7 | 66.9 | 95.4 |
| 50Si/PyC/CNF:NG=2:8 | 72.1 | 96.7 |
| 50Si/PyC/CNF:NG=1:9 | 77.8 | 98.8 |
| NG | 90.0 | 106.9 |

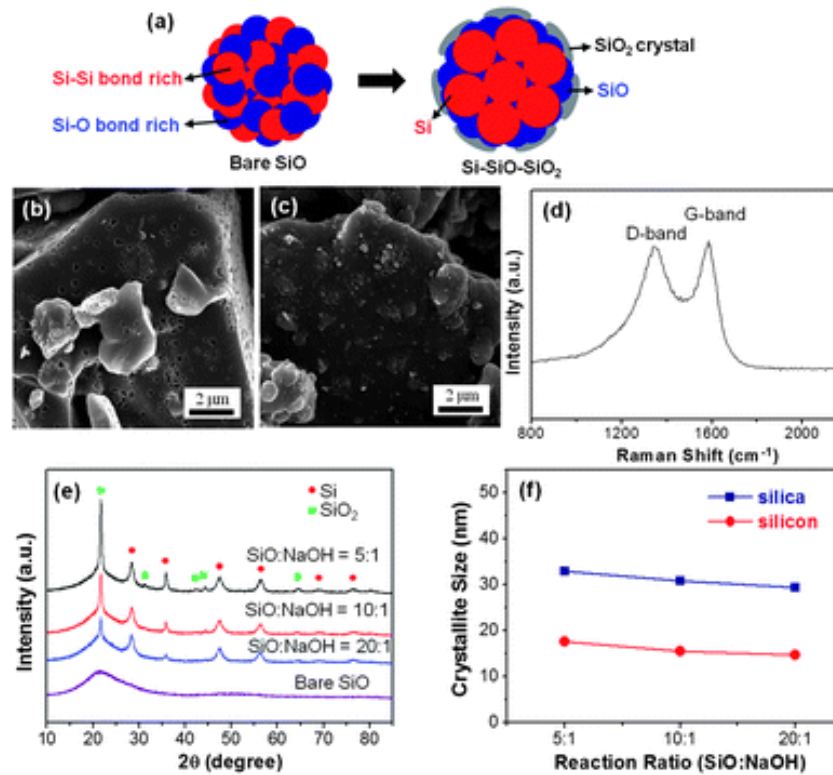
✓ The hybrids of the Si/PyC/CNF and NG showed better cycle-ability than the hybrids of Si/PyC and NG.

Highly stable Si-based multicomponent anodes for practical use in lithium-ion batteries

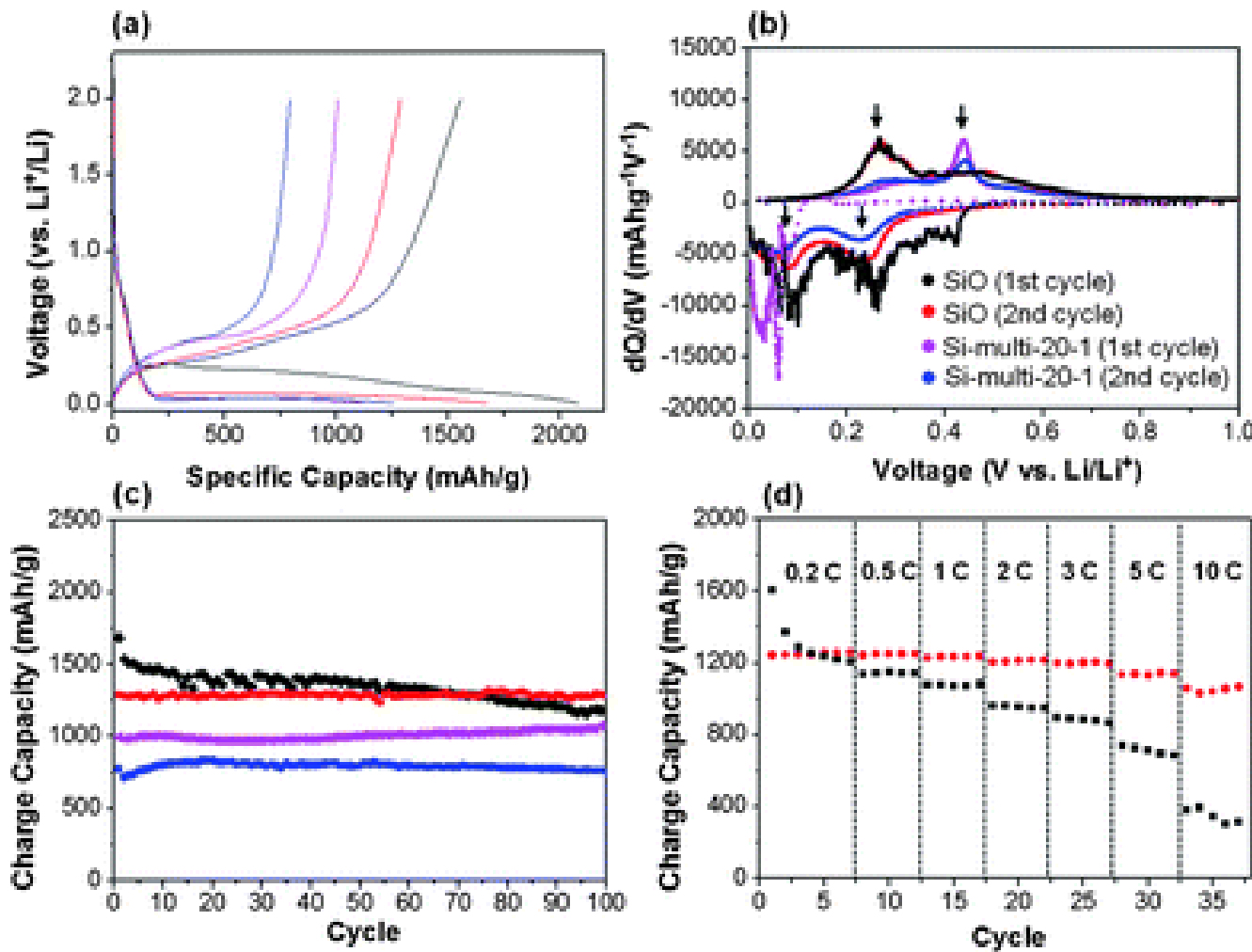
Jung-In Lee , Nam-Soon Choi and Soojin Park

Energy Environ. Sci., 2012, 5, 7878-7882

Interdisciplinary School of Green Energy, Ulsan National Institute of Science and Technology, Ulsan, Korea 689-798



Synthesis of an Si-based multicomponent from bulk SiO particles via thermal annealing in the presence of NaOH. (a) Schematic illustration for the conversion of bare SiO to Si–SiO–SiO₂ three-components, (b) SEM image of Si-based multicomponents, SEM image (c) and Raman spectrum (d) of carbon-coated Si-based multicomponents, (e) XRD patterns of Si-based multicomponents as a function of NaOH amount, and (f) calculation of silica and silicon crystallite size as a function of NaOH amount



Electrochemical performances of c-SiO and c-Si-SiO-SiO₂ three-component electrodes. (a) Voltage profiles of c-SiO (black), c-Si-multi-20-1 (red), c-Si-multi-10-1 (pink), and c-Si-multi-5-1 (blue). (b) dQ/dV plots of c-SiO and c-Si-multi-20-1 (red) in the first and second cycles. (c) Cycle performances of c-SiO (black), c-Si-multi-20-1 (red), c-Si-multi-10-1 (pink), and c-Si-multi-5-1 (blue) at 0.1 C rate. (d) Rate capabilities of c-SiO and c-Si-multi-20-1 electrodes. The discharge rate was fixed at a rate of 0.1 C

まとめ

- Bulk Carbon以外は、長所と共に短所も持っております、まだLi-ion電池用負極としては商品化されていない。
- 今後の研究によって短所が解決できれば、電池の特性はより改善できる。